To what extent are greenhouse-gas emissions offset by trees in a Sahelian silvopastoral system?

Yélognissè Agbohessou, Claire Delon, Eric Mougin, Manuela Grippa, Torbern Tagesson, Moussa Diedhiou, Seydina Ba, Daouda Ngom, Rémi Vezy, Ousmane Ndiaye, et al.

Agricultural and Forest Meteorology 343 (2023) 109780

Contents lists available at ScienceDirect

Agricultural and Forest Meteorology

journal homepage: www.elsevier.com/locate/agrformet

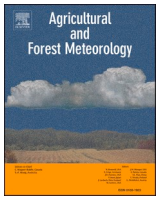

To what extent are greenhouse-gas emissions offset by trees in a Sahelian silvopastoral system?

Yélognissè Agbohessou [a,b,c,*], Claire Delon [d], Eric Mougin [e], Manuela Grippa [e], Torbern Tagesson [f,g], Moussa Diedhiou [a], Seydina Ba [a,c], Daouda Ngom [a], Rémi Vezy [h,i], Ousmane Ndiaye [b,j], Mohamed H. Assouma [k,l], Mamadou Diawara [m], Olivier Roupsard [c,n,o]

[a] Université Cheikh Anta Diop, Dakar, Senegal
[b] Institut Sénégalais de Recherches Agricoles, Dakar, Senegal
[c] LMI IESOL, Centre IRD-ISRA de Bel Air, Dakar, Senegal
[d] Laboratoire d'Aérologie, Université de Toulouse, CNRS, UPS, Toulouse, France
[e] Géosciences Environnement Toulouse, Université de Toulouse, CNES, CNRS, IRD, UPS, Toulouse, France
[f] Department of Geosciences and Natural Resource Management, University of Copenhagen, Copenhagen, Denmark
[g] Department of Physical Geography and Ecosystem Science, Lund University, Sölvegatan 12, S-223 62, Lund, Sweden
[h] CIRAD, UMR AMAP, F-34398 Montpellier, France
[i] AMAP, Univ Montpellier, CIRAD, CNRS, INRAE, IRD, Montpellier, France
[j] Centre de Recherche Zootechniques de Dahra, Institut Sénégalais de Recherche Agricoles, Dakar, Senegal
[k] SELMET, University of Montpellier, CIRAD, INRA, Montpellier SupAgro, Montpellier, France
[l] International Center for Research and Development on Livestock in Subhumid Regions (CIRDES), Bobo-Dioulasso, Burkina Faso
[m] Département de Biologie, Faculté des Sciences et Techniques (FST), Université des Sciences, des Techniques et des Technologies de Bamako (USTTB), Colline de Badalabougou, B.P. 3206 Bamako, Mali
[n] CIRAD, UMR Eco&Sols, Dakar, Senegal
[o] Eco&Sols, Univ Montpellier, CIRAD, INRAE, Institut Agro, IRD, Montpellier, France

ARTICLE INFO

Keywords:
Silvopastoral systems
Greenhouse gas emissions
Livestock
Trees
Process-based model

ABSTRACT

To assess the extent to which trees in a semi-arid silvopastoral system (SPS) can offset the greenhouse-gas (GHG) emissions of the system's livestock, this study used two process-based models (STEP-GENDEC-N_2O and DynACof) to simulate 9 years of agricultural activity and resulting emissions in a SPS that has been operating in sahelian Senegal. STEP-GENDEC-N_2O simulated soil N_2O and CO_2 fluxes, plus growth of the herbaceous layer, while DynACof focused on the tree layer. Outputs from the models included simulated time series of vegetative growth, water fluxes, and emissions. This output was validated through the use of published data, and measurements that were made at the SPS. Overall, the outputs from STEP-GENDEC-N_2O agreed well with validation data for water fluxes, soil N, soil C, herbaceous biomass, and N_2O emissions. Good agreement was also found between the measured fluxes of the SPS ecosystem, and the simulated values that were generated by combining STEP-GENDEC-N_2O's simulations (of the herbaceous layer's heterotrophic respiration, autotrophic respiration, and gross primary productivity (GPP)) with DynACof's simulations of the tree layer's autotrophic respiration and GPP. Among the insights gained from the simulations was that in this SPS's sandy soils, nitrification was the dominant process that leads to N_2O emissions. Our results show that the trees, at their current density (81 ha^{-1}) offset 18 % to 41 % of the GHG emissions from livestock. With further development, the model set-up can be used for estimating the GHG offset at other tree densities, and will be useful for guiding future policies regarding climate-change adaptation and mitigation in the management of the Sahel's SPSs.

1. Introduction

The impacts of climate change are becoming increasingly evident in ecosystems worldwide. Greenhouse gas (GHG) emissions negatively impact air, soil and water quality at the global scale (IPCC, 2022). In recent years, numerous research efforts have been dedicated to

* Corresponding author at: Université Cheikh Anta Diop, Dakar, Senegal.
E-mail address: yelognissefredi.agbohessou@ucad.edu.sn (Y. Agbohessou).

https://doi.org/10.1016/j.agrformet.2023.109780
Received 10 January 2023; Received in revised form 12 October 2023; Accepted 21 October 2023
Available online 25 October 2023

exploring this issue from local to global perspectives across the world (IPCC, 2022; Parmesan et al., 2022; Pörtner et al., 2022). Nevertheless, a significant portion of our understanding regarding the scale of GHG emissions, their impacts, and climate risks in Africa predominantly relies on evidence from global studies (Tian et al., 2020; Zhao et al., 2021). While these global studies provide estimates of average global trends, they may not possess the statistical power to distinguish the specific magnitudes of GHG emissions, vulnerability, exposure, or adaptation capacity within African ecosystems (Trisos et al., 2022). More localized studies in Africa can further enhance our comprehension of climate change impacts on the continent.

According to the Intergovernmental Panel on Climate Change's (IPCC) sixth assessment report (2022), Africa is the continent that contributes least to global GHG emissions. At the same time, Africa has been and is projected to continue being the continent most impacted by climate change. Key development sectors in Africa have already experienced widespread damages attributable to anthropogenic climate change, including biodiversity loss, water shortages, reduced food production, loss of life, and slower economic growth (Trisos et al., 2022). For example, recent studies in Senegal have demonstrated both the vulnerability of ecosystems to climate change, and the need to adapt practices to predicted future climates in order to mitigate potential impacts upon food production (Ministère de l'Environnement, du Développement durable et de la Transition écologique du Sénégal, 2015). Senegal has responded by proposing a set of strategies for reducing its GHG emissions. Proposals for its agriculture sector promote sustainable land-management technologies (Ministère de l'Environnement, du Développement durable et de la Transition écologique du Sénégal, 2015). To inform the policies for developing and implementing those technologies, Senegal needs estimates of the magnitudes of direct agricultural GHG emissions, along with knowledge of the biophysical controls upon those emissions. Such information is especially important regarding Senegal's semi-arid savannas, which are a dominant vegetation type in that nation (Latham et al., 2014). Within those savannas, one of the typical land use types is the Sahelian silvopastoral system (SPS).

SPSs are complex systems in which livestock graze within a mix of trees and pastures. The ecosystem services that are provided by SPSs include biodiversity conservation (Newbold et al., 2015), carbon sequestration in vegetation and soils (Chapman et al., 2020), and cooling due to trees (Zeppetello et al., 2022). According to Montagnini et al. (2013) and Torres et al. (2017), the use of silvopastoral systems can adapt the Sahelian region to climate change, while simultaneously providing food and livelihoods for millions of people (Godde et al., 2020). An unresolved issue regarding SPSs is the net impact of the associated livestock upon climate. Livestock affect the carbon (C) cycle and GHG fluxes strongly (Butterbach-Bahl et al., 2020), mainly through grazing and the excreta that increase soil fertility by recycling carbon (C) and nitrogen (N) to the system. However, livestock also increase emissions of N_2O and CO_2 (Dangal et al., 2020). Although those processes are well known, the extent to which they operate in SPSs is poorly understood, as are the magnitudes of their potential impacts.

To quantify such impacts (more specifically, a region's contribution to the global carbon budget), experts often use global dynamic vegetation models (Tian et al., 2015). Unfortunately, those models do not always represent the unique characteristics of sub-Saharan ecosystems with sufficient accuracy. Despite the efforts made by some authors to measure the region's GHG emissions, the sources and magnitudes of those emissions remain highly uncertain. To our knowledge, very few experimental studies have focused upon estimating GHG emissions from SPSs, or upon identifying their driving parameters. Most of the published studies measured GHG emissions by using static chambers placed over the soil surface (Assouma et al., 2017; Bigaignon et al., 2020; Delon et al., 2017). These studies provided only snapshots of emissions, typically with coarse temporal resolutions. What are needed, in addition, are long-term studies with the temporal resolutions that are required for satisfactory modeling (Bentzon-Tarp et al., 2023). Temporal resolution is especially important for measurements that are made during the transition period between the Sahel's dry and the wet seasons. During those periods, GHG emissions are expected to peak after the first rains fall upon very dry soils (Assouma et al., 2017). Unfortunately, field measurements of soil GHG emissions are expensive, time-consuming, and labour-intensive especially in African SPSs, which are usually located in remote areas with little or no infrastructure. As an important alternative, process-based modeling can complement the few available experimental studies, thereby providing insights into the underlying processes of GHG emission, as well as the temporal and spatial variability of GHG fluxes.

Studies that have been carried out in temperate regions are instructive regarding the processes that might need to be modeled, and the parameters to be included. Several of those studies found that CO_2 and N_2O emissions from soils result from biogeochemical processes that are related directly or indirectly to the activity of soil microorganisms (Firestone and Davidson, 1989; Knowles, 1982; Robertson and Paul, 2000; Ward, 2013). Specifically, the CO_2 is generally produced during decomposition of soil organic matter (Robertson and Paul, 2000), while N_2O emissions are derived predominantly from denitrification (i.e., reduction of nitrate to molecular N) and nitrification (i.e., oxidation of ammonium to nitrate) (Davidson and Verchot, 2000). The activation of the microorganisms responsible for these processes depends upon a range of environmental factors, the most important of which are soil water content, substrate concentration gradient, soil pH, and temperature (Aulakh et al., 1991; Bajracharya et al., 2000; Reth et al., 2005). The key ecological drivers of these factors are climate, soil properties, vegetation, and anthropogenic activities (Li, 2007). Any change in these ecological drivers may cause changes in the environmental factors that affect the processes through which CO_2 and N_2O are produced and consumed in the soil (Li, 2007). Because the complexity of these relationships cannot be described with simple empirical models, process-based models are the most convenient tool for studying, quantifying, and predicting how a change in ecological drivers might affect emission of CO_2 and N_2O.

The need for modelers to take context-specific ecological dynamics into account has motivated recent modeling efforts that incorporate simulations of semi-arid climate conditions. Especially important is the accurate representation of strong changes in soil C and N dynamics that occur during the transition between the dry and wet seasons (Bigaignon et al., 2020; Delon et al., 2019). In the case of models that attempt to describe the processes leading to CO_2 and N_2O production in SPSs, it is also necessary to improve the parameterization of ecological processes that operate in the Sahel's specific combination of high temperatures, long dry seasons, low annual precipitation, and effects of livestock and trees.

To address that need, this study examines the processes through which the trees in a SPS offset the emissions of CO_2, N_2O, and CH_4 emissions that result from the livestock. We also make quantitative predictions of the offsets. The specific research questions are: (1) What are the annual CO_2 and N_2O balances of a typical SPS in the Western Sahel; (2) How are the CO_2 fluxes distributed between herbaceous vegetation and trees; and (3) What is the impact of livestock, and how could the livestock-related emissions of CO_2, N_2O, and CH_4 be offset?

2. Materials and methods

2.1. Study area

The study area is a Sahelian SPS at the Dahra field site in northwestern Senegal (15°24′10″N, 15°25′56″W, elevation 40 m, Fig. 1(a)). The site lies within the Centre de Recherches Zootechniques, which is managed by the Institut Sénégalais de Recherche Agronomique (ISRA). The site is equipped with an Eddy Covariance (EC) tower (Fig. 1(b)) (Tagesson et al., 2015, 2016b). The climate is Sahelian, with a unimodal

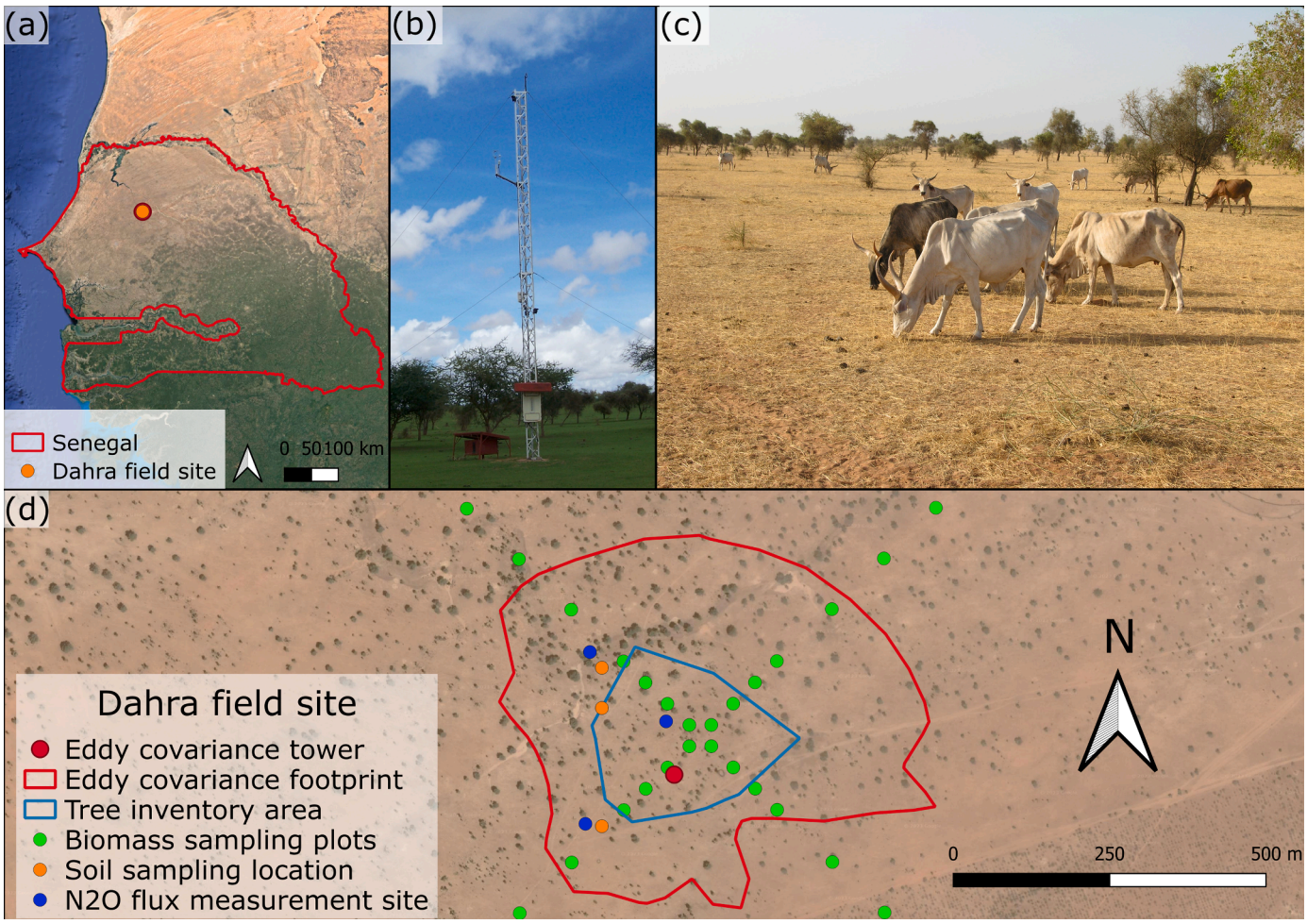

Fig. 1. The study area (Dahra field site, Senegal): (a) location of the site (15°24′10″N, 15°25′56″W); (b) photograph of the eddy covariance (EC) tower, taken during the wet season; (c) photograph of the Dahra landscape, showing livestock, dry herbaceous vegetation, and trees; (d) closeup of the Dahra field site, showing locations of sampling and instrumentation.

rainfall pattern that features a wet season extending from July to October. During 2012–2020, the mean annual precipitation was 380 mm (range: 271–529 mm), and the mean annual air temperature was 28.9 °C (range: 28–30 °C).

Soils in the study area are sandy (89 % sand, 6.3 % clay). Within the upper soil profile, pH_{H2O} ranges from 6.2 to 7.4 (Delon et al., 2022). The site is a typical unmanaged SPS, with a sparse tree population (6.4 % canopy cover) (Tagesson et al., 2015). The dominant tree species is *Acacia raddiana and Balanites aegyptiaca;* also present are *Acacia senegal* and *Leptadenia astata.* Herbaceous vegetation consists primarily of annual C4 grasses (*Dactyloctenium aegyptum, Aristida adscensionis, Cenchrus biflorus* and *Eragrostis tremula*), which are grazed year-round by cows (*Bos taurus indicus*) (Fig. 1(c)), sheep (*Ovis aries*), and goats (*Capra aegagrus hircus*) (Tagesson et al., 2015). The site's high grazing pressure (approximately 242 to 1210 grazing animals on a 500-ha service area) is about 4 times greater than the average pressure in the Sahel (Gilbert et al., 2018). The site is described in greater detail by Tagesson et al. (2015, 2016b) and Delon et al. (2022, 2019, 2017).

2.2. Field data

2.2.1. Hydro-meteorological and flux data

The hydro-meteorological data used for this study were rainfall (mm); air temperature (°C), relative air humidity (%); wind speed (m s^{-1}) at 2 m height; soil moisture (m^3 m^{-3}) at depths of 0.05, 0.10, and 0.30 m; and net radiation (W m^{-2}). These data were measured during the period 2012–2020 at the meteorological station of the Dahra field site by sensors that were connected to a CR-1000 logger in combination with a multiplexer (Campbell Scientific Inc. North Logan, USA) (Tagesson et al., 2015). Data were sampled every 30 s and integrated for storage every 15 min. CO_2 and latent heat fluxes were measured at a height of 9 m above ground level at a frequency of 20 Hz, using an eddy covariance-system consisting of a CO_2/H_2O infrared gas analyzer (2010–2017: open-path LI-7500, LI-COR Inc., Lincoln, USA; 2019–2020: enclosed path EC155 Campbell Scientific Inc. North Logan, USA) and a three-axis sonic anemometer (2010–2017: Gill R3 ultrasonic anemometer, Hampshire, UK; 2019–2020: CSAT3A, Campbell Scientific Inc. North Logan, USA). Post-processing was performed with the EddyPro 4.2.1 software (Li-Cor Biosciences, 2012). Statistics were calculated for 30-min periods (Tagesson et al., 2015). All data were integrated at the daily scale. The methods that were used for quality checks, gap-filling, and partitioning of the measured NEE (Net Ecosystem Exchange) fluxes into gross primary production and ecosystem respiration (R_{eco}) were based upon previous work (Tagesson et al., 2016a).

N_2O emissions were measured at three different locations below the flux tower, at the top, midpoint, and bottom of a 500 m transect along a dune slope of 2 % (nearly flat). The herbaceous vegetation cover in the field is rather homogeneous, thus ensuring that the soil cover inside the chamber is representative of the area (Fensholt et al., 2006; Fensholt and Sandholt, 2005). N_2O emissions were measured three times a day (morning: 10–12 am; noon: 12 am–2 pm; and afternoon: 04–06 pm) during three field campaigns (11-07-2013 to 17-07-2013, 29-10-2013 to

07-11-2013, and 21-09-2017 to 27-09-2017) using a stainless-steel chamber (base: 0.20 m × 0.40 m, height: 0.15 m). The chamber was placed on a frame inserted 10 cm deep in the soil, and sealed by a water-filled slot (Bigaignon et al., 2020; Delon et al., 2017). Samples of the chamber headspace gas were then extracted with a syringe through a rubber septum. During 2013, the samples were extracted at 0, 15, 30, and 45 min after placing the chamber on the frame. During 2017, the times of extraction were 0, 20, 40, and 60 min. Samples were transferred into 12 mL pre-evacuated glass vials (Exetainer, Labco, UK). Two to three weeks after each field campaign, the gas samples were analyzed via gas chromatography (GC) at Laboratoire d'Aérologie, (Toulouse, France) (Bigaignon et al., 2020; Delon et al., 2017). The gas chromatograph (SRI 8610C; from SRI, Torrance, CA, USA) was equipped with an electron capture detector (ECD). N_2O fluxes were calculated from the slope of the linear regression of gas concentration in the chamber versus time (Assouma et al., 2017; Delon et al., 2017). Previous publications that used these data (Bigaignon et al., 2020; Delon et al., 2017) present a full description of the method that was used, as well as the quality checks of measured N_2O emissions.

2.2.2. Data for soil, vegetation, and trees

Soil samples were collected during 2015–2020 at the top, mid-point, and bottom of a 500-m transect that followed a dune slope (Fig. 1(d)). The samples were collected with a core sampler at depths of 0–10 cm, 20–30 cm, 30–40 cm, and 50–60 cm. After air-drying, the samples were analysed (for soil properties) by the « Laboratoire des Moyens Analytiques » (UAR IMAGO—LAMA certified ISO9001:2015), at Dakar's IRD (« Institut de Recherche pour le Dévelopement ») (http://www.imago.ird.fr/moyens-analytiques/dakar). Organic carbon was determined using the method of Walkey and Black (1934). pH was measured on soil samples that had been stirred with water (1/2.5 w/v). Total C and N contents were determined by a CHN elemental analyzer (Thermo Finnigan Flash EA1112, Milan, Italy) using the Dumas method (Stewart et al., 1963) on 100 mg aliquots that had been ground to 0.2 mm. The determinations were made according to ISO 10694:1995 (for C) and ISO 13878:1998 (for N).

Samples for calculation of total above-ground herbaceous mass were collected during the 2013–2019 wet seasons, at intervals of approximately 10 days. The samples were taken from twenty-eight 1-m^2 plots located along two 1060-m long transects (Fig. 1(d)) (Mbow et al., 2013; Tagesson et al., 2015). During 2020, herbaceous-vegetation samples were collected every 2 days from July 19th to September 17th, in 1 m^2 plots at three different locations near a tree on the plot (under the crown; at the crown edge and far from the crown). The collected herbaceous vegetation was weighed in the field to find the fresh weight. The dry matter was estimated by oven-drying the green biomass for 48 h. A more detailed description of the biomass-sampling method can be found in Mbow et al. (2013).

A systematic inventory of the tree population at the site was carried out on 10/11/2022 over a 4-ha area around the EC tower (Fig. 1(d)). The following parameters were recorded: species name, tree height; tree circumference; and crown diameters (measured in the two largest perpendicular directions). Biomasses of wood and leaves were calculated using allometric equations found in the literature (Cissé, 1980; Hiernaux et al., 2022; Poupon, 1980). Details about the measured structural parameters of the trees can be found in Table A.1. The allometric equations used to calculate the wood and leaf biomasses of trees are in Table A.2.

2.2.3. Dataset

Meteorological data: Additional climatic data (1990 to 2011) required for simulations were derived from NASA's POWER (Prediction Of Worldwide Energy Resources) dataset (Stackhouse et al., 2018). The meteorological data collected were air temperature (°C), rainfall (mm), wind speed (m s^{-1}), relative air humidity (%), global radiation (MJ m^{-2}), and photosynthetically active radiation (MJ m^{-2}). These data were based upon products from the Goddard's Global Modeling and Assimilation Office (GMAO) Modern Era Retrospective-Analysis for Research and Applications (MERRA-2) assimilation model. NASA's POWER data have already been widely used in several modeling studies (Ojeda et al., 2017; Savary et al., 2012; Van Wart et al., 2015). Uncertainty estimates of the dataset are based upon comparisons with surface measurements. Validation results can be found in White et al. (2011, 2008).

N_2O and CH_4 Tier 1 data: N_2O emissions from manure and CH_4 emissions from enteric fermentation (CO_2eq) were derived from FAOSTAT domain Emissions (FAOSTAT, 2022). Such data are computed at Tier 1 of the IPCC Guidelines for National greenhouse gas (GHG) Inventories (IPCC, 2006). Annual estimates of N_2O emissions from manure were extracted for the period 2012–2019, as were CH_4 emissions from enteric fermentation in Senegal. Using the area of Senegal, the data for the whole country were downscaled to CO_2 eq ha^{-1} to calculate the emissions at the Dahra field site. Fluxes were converted to CO_2 equivalents using the 100-year global warming potential (IPCC, 2014).

2.3. STEP-GENDEC-N_2O

2.3.1. Model description

STEP-GENDEC-N_2O is a 1D coupled, process-based model developed for Sahelian herbaceous savannas (Bigaignon et al., 2020; Delon et al., 2019; Moorhead and Reynolds, 1991; Mougin et al., 1995). It simulates a set of processes that describe the cycling of water, C, and N between the atmosphere, vegetation, and soil at a 1-day temporal resolution. Specifically, the STEP model simulates the water budget and herbaceous vegetation growth (Mougin et al., 1995). GENDEC then simulates the dynamics of microbial activity and the decomposition of buried litter (Moorhead and Reynolds, 1991). The N_2O emission module from Bigaignon et al. (2020) simulates the N_2O emissions from nitrification and denitrification processes. STEP-GENDEC-N_2O model is forced daily by rain, global radiation, air temperature, wind speed, and relative air humidity at 2 m height.

In the STEP model, the amount of the water infiltration into the soil profile is determined from rainfall intensity (at the daily scale) and the soil's surface characteristics. The soil water is distributed within four soil layers (0–2 cm, 2–30 cm, 30–100 cm and 100–300 cm) according to a tipping bucket scheme (Manabe, 1969). Soil water contents at field capacity and at the wilting point are derived as a function of soil texture (Delon et al., 2019). Actual soil evaporation and plant transpiration are simulated following the Penman Monteith approach (Monteith, 1965). Vegetation plays a strong role in the water budget through the plants' interception and transpiration of water, as well as by reducing evaporation from the soil surface. For each vegetation component, the STEP model calculates the associated cover fraction via an equation that is based upon the Beer-Lambert law of light extinction. The calculation takes into account the corresponding Leaf Area Index (LAI) (Mougin et al., 2014). The proportion of bare soil exposed to solar radiation (=1 the total ground-cover fraction) is used to calculate soil evaporation and (indirectly) soil water content. The soil C content is calculated from the total litter input, while soil N is derived from the quantity of C and the litter's C/N ratio (Delon et al., 2015). In other words, the model assumes that C and N are added to the soil's existing stocks via decomposition (by soil microflora and microfauna) of litter that was incorporated into the profile through (for example) trampling by livestock. Inputs might also occur through the actions of insects and small animals.

Aboveground and belowground plant respiration was partitioned into amounts for growth and maintenance. As inputs for simulating microbial respiration, GENDEC used STEP's values of soil moisture, soil temperature, and biomass (i.e., herbal mass, herbaceous root mass, ligneous, and fecal matter from livestock). N_2O productions and emissions from nitrification and denitrification were simulated using DNDC's (DeNitrification-DeComposition) equations (Li, 2000; Liu, 1996), adapted to the semi-arid region as described in Bigaignon et al. (2020).

For the denitrification process, the threshold value of water-filled pore space (WFPS) i.e., the ratio of volumetric soil water content to total soil porosity was set to 26 %.

2.3.2. Model setup and initialization

The STEP-GENDEC-N_2O model simulated a nine-year period (2012–2020). This simulation was preceded by a 6-year spin-up time to allow the carbon and nitrogen pools to stabilise. The soil conditions, vegetation state, and animal load used for initialising the model are detailed in Table A.1. The other initial parameter values were retrieved from previous studies that ran the model for the same site (Bigaignon et al., 2020; Delon et al., 2019).

The main model parameter values and equations used for nitrification and denitrification can be found in Tables A.4 to A.7 of the Appendix. To recalculate the cover fraction associated with each vegetation component (green, dry, and litter), the model adapted an equation that Mougin et al. (2014) developed for estimating vegetation cover fractions in Mali. This equation is based upon Beer-Lambert's law of light extinction, taking into account the corresponding LAIs of green and dry vegetation.

$$fCover_g = 1 - exp\left(-0.431 * LAI_g\right) \quad (1)$$

$$fCover_d = 0.75 - exp(0.319 * LAI_d) \quad (2)$$

$$fCover_i = 0.5 - exp\left(0.069 * LAI_g\right) \quad (3)$$

$fCover_g$, $fCover_d$, and $fCover_i$ are respectively the cover fractions for green biomass, dry biomass, and litter biomass. LAI_g and LAI_d are respectively the LAI of green and dry vegetation.

2.4. DynACof

2.4.1. Model description

DynACof is a generic, open-source (https://vezy.github.io/DynACof/) tree-growth model that was developed (initially) to simulate the growth, yield, C balances, and water balances of one or two layers of perennial plants. Its original application was to coffee grown in plantations–either as a monoculture, or under a sparse top layer of trees in agroforestry systems (Vezy et al., 2020). DynACof is 1-D, with a one-day time step. The model is generic for perennials, and includes a pruning module that can be adjusted to simulate local conditions. In this study, we adapted the top-layer (shade-tree) module specifically to simulate the Dahra site's sparse tree canopy, which is dominated by *A. raddiana* and *B. aegyptiaca*. We simulated each of these species separately, then summed the results to find the values for the entire tree layer. The following were simulated at a one-day time step: tree layer autotrophic respiration, net primary productivity (NPP), gross primary productivity (GPP), and mortality of the tree components (leaves, branches, stems, and roots). A more detailed description of the model can be found in Vezy et al. (2020).

2.4.2. Model setup and initialization

DynACof was run for a simulated thirty-year period (1990–2020). We chose that duration based upon local testimony and the assumption that the average tree at the site is at least thirty years old. (No dendrochronological data is available.) The meteorological data for driving the model during 1990–2011 (i.e., air temperature, rainfall, global radiation, wind speed, relative air humidity, and photosynthetically active radiation) were derived from NASA's POWER dataset (Stackhouse et al., 2018). Meteorological data for 2012 to 2020 were from measurements at the Dahra field site. The tree density at the site is 29 trees ha^{-1} for *A. raddiana* and 52 trees ha^{-1} for *B. aegyptiaca*. Trees are pruned frequently to feed livestock during the dry season usually just before the wet season starts. According to local testimony, *B. aegyptiaca* is the main species being pruned. The parameter values used for adapting the model are detailed in Table A.2.

Our simulation of litter inputs from trees was based upon the observation that dead branches are exported from the site and used for firewood. Thus, the trees' contribution to soil organic matter consists of dead leaves and tree roots. In our simulation, STEP-GENDEC-N_2O used each year's simulated annual production of that material as an input at the beginning of the following year (Appendix B, Fig. B.1). This practice allowed us to account for the contribution of tree litter to the total soil organic carbon in STEP-GENDEC-N_2O. Then, to quantify the subsequent year's CO_2 flux distribution between tree and herbaceous vegetation, and to calculate the ecosystem's CO_2 flux, we combined the tree autotrophic respiration and GPP (as simulated with DynACof) with R_{eco} and GPP (as simulated with STEP-GENDEC-N_2O). We computed the tree NEP (Net Ecosystem Production: the total amount of C stored in trees yr^{-1}) as:

$$NEP_{Tree} = GPP_{Tree} - Ra_{Tree} - Rh_{Tree} - \left(Branche_{Exports} + Stem_{Exports}\right) \quad (4)$$

where NEP_{Tree} (tC ha^{-1} yr^{-1}) is the trees' contribution to ecosystem NEP; GPP_{Tree} is the tree layer's GPP; Ra_{Tree} is the tree layer's autotrophic respiration; Rh_{Tree} is the heterotrophic respiration due to the decomposition of tree litter; and $Branche_{Exports}$ and $Stem_{Exports}$ are respectively the amounts of carbon in the tree branches and stems that are exported from the site.

2.4.3. Model calibration

A multi-objective calibration approach was used when adapting the model to *A. raddiana* and *B. aegyptiaca*. We calibrated the trees' GPP, R_a and transpiration with EC measurements from the second-half of the dry-season. The reason for this choice of calibration is that during that period, there is no herbaceous vegetation at the site, and the soil is extremely dry. Therefore, we assumed that the soil's contribution to evaporation and respiration was negligible at that time. The leaf and wood biomass simulated by DynACof were validated for each tree species with biomass calculated from measured data, using allometric equations found in the literature (Fig. B.4 and Table A.3).

2.5. Models' boundaries

We assumed that livestock affect only the inputs of C and N to the soil. Transhumance was not simulated. The STEP-GENDEC-N_2O model takes into account the C and N inputs to soil from the livestock's feces, and from the litter that livestock incorporate into the soil profile via trampling. The incorporation of that material facilitates mineralization of N, but STEP-GENDEC-N_2O does not simulate the expected enhancement of vegetation growth. Therefore, the model may underestimate the grass's GPP. STEP-GENDEC-N_2O includes the trees' above- and belowground litters, which participate in soil heterotrophic respiration and N_2O emissions. However, CH_4 emitted directly by the livestock are not simulated. DynACof simulates sparse trees and accounts for pruning, but is not limited by availability of N and water. We assumed that trees are deeply rooted and access deep water resources.

2.6. Summary of the modeling workflow

We first calibrated the water and C balances in STEP-GENDEC-N_2O, whose DynACof model had been adapted previously to simulate CO_2 fluxes of tree layers. Next, we improved the parameterization of N_2O emissions in STEP-GENDEC-N_2O. Lastly, we estimated the impact of livestock upon ecosystem GHG emissions, and computed the trees' offsetting potential. We also conducted an uncertainty analysis (UA) via Monte Carlo simulation (MCS), as well as a sensitivity analysis (SA) using Sobol's method (Sobol, 2001) (See appendix C for details).

2.7. Statistical analysis

The "goodness of fit" of the model's predictions was assessed by calculating the model efficiency (EF), the root mean square errors (RMSEs), and the mean predictive error (BIAS). EF (also known as the Nash-Sutcliffe efficiency (NSE)) assesses the model's predictive ability. EF is calculated as one minus the ratio of the error variance of the modeled time-series, divided by the variance of the observed time-series. For a perfect model with an estimation-error variance equal to zero, the EF equals 1 (Vezy et al., 2021). RMSE assesses the accuracy of the model, while BIAS measures the absolute differences between observations and the simulated values.

3. Results

3.1. Soil water content (SWC) and evapotranspiration (ET)

Simulated SWC ranged from 3 % (the wilting point) to 15 % (field capacity). The model represents seasonal dynamics of the SWC quite well over the entire study period (Fig. 2(a) and (c): EF = 0.67, RMSE = 1.38 %, and BIAS = 0.19). At the end of the 2014 wet season, the simulated SWC decreased more rapidly than the observed SWC, but decreased more slowly in 2017.

Seasonal dynamics of daily ET are also represented well by the model (Fig. 2(b)), which explains 65 % of the daily ET variability (Fig. 2(d)). Although the model tends to underestimate high ET rates (Fig. 2(d):

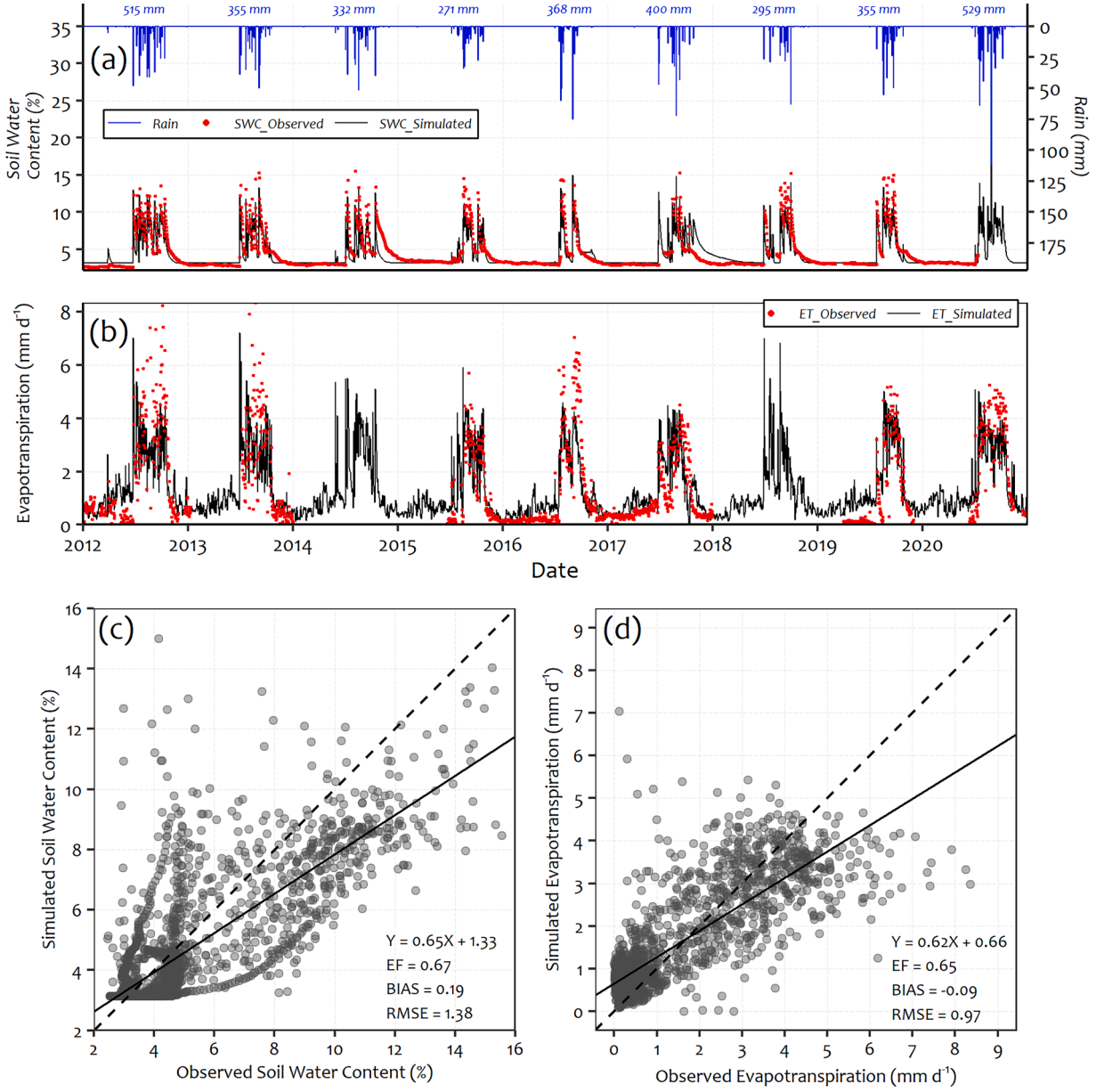

Fig. 2. Time series (2012–2020) of the simulated and observed SWCs and evapotranspiration. In (a), the blue lines show daily precipitation in mm d^{-1}. Blue numbers at the top of the graph are total annual precipitations. The black line in (a) shows the simulated SWCs for the 2–30 cm layer (per STEP-GENDEC-N_2O). The red dots show the observed values of SWC at the 10 cm depth. In (b), the black line shows the simulated evapotranspiration (from STEP-GENDEC-N_2O). Red dots indicate the evapotranspiration values that were measured via EC. In the scatter plots shown in (c) and (d), the thick black lines are from the respective linear regressions, and the dashed black lines are 1:1 lines. The scatter plot in (c) compares the SWC (%) of the 2–30 cm layer as simulated by STEP to the SWC measured at 10 cm. In (d), the ET (mm d^{-1}) simulated by STEP is compared to the actual evapotranspiration measured by EC. (For interpretation of the references to color in this figure legend, the reader is referred to the web version of this article.)

slope = 0.62 and BIAS = −0.09 mm), there is good overall agreement between simulated and observed daily ET throughout the study period (Fig. 2(d): EF = 0.65, RMSE = 0.97 mm d^{-1}).

3.2. Herbaceous aboveground biomass (AGB), and the soil C and N

Simulated values of the herbaceous AGBs agree well with field observations (Fig. B2(a)), even though the AGB is overestimated for the years 2013–2015.

Ranges of the values from the simulation are consistent with those of the measurements, although the model underestimated soil C in 2018 and 2020 (Fig. B2(b)). Similar dynamics of soil C content were found at the Dahra site by Elberling et al. (2003b, 2003a). Simulated soil C and N contents exhibited seasonal fluctuations, peaking in the middle of the dry season and decreasing at the end of the wet season. These fluctuations highlight a rapid soil C turnover due to short term decomposition processes (Moorhead and Reynolds, 1991). This result is consistent with the observation that during the course of the rainy season, the soil's C content is reduced by decomposition of litter. The C content is then replenished with new buried litter at the beginning of the next dry season. The average measured and simulated soil C contents are 0.27 ± 0.03 % and 0.23 ± 0.02 %, respectively. The average N content from the simulation (0.02 %) is equal to the measured value, although the uncertainties are slightly different (simulated = ±0.001 %; measured = ±0.002 %).

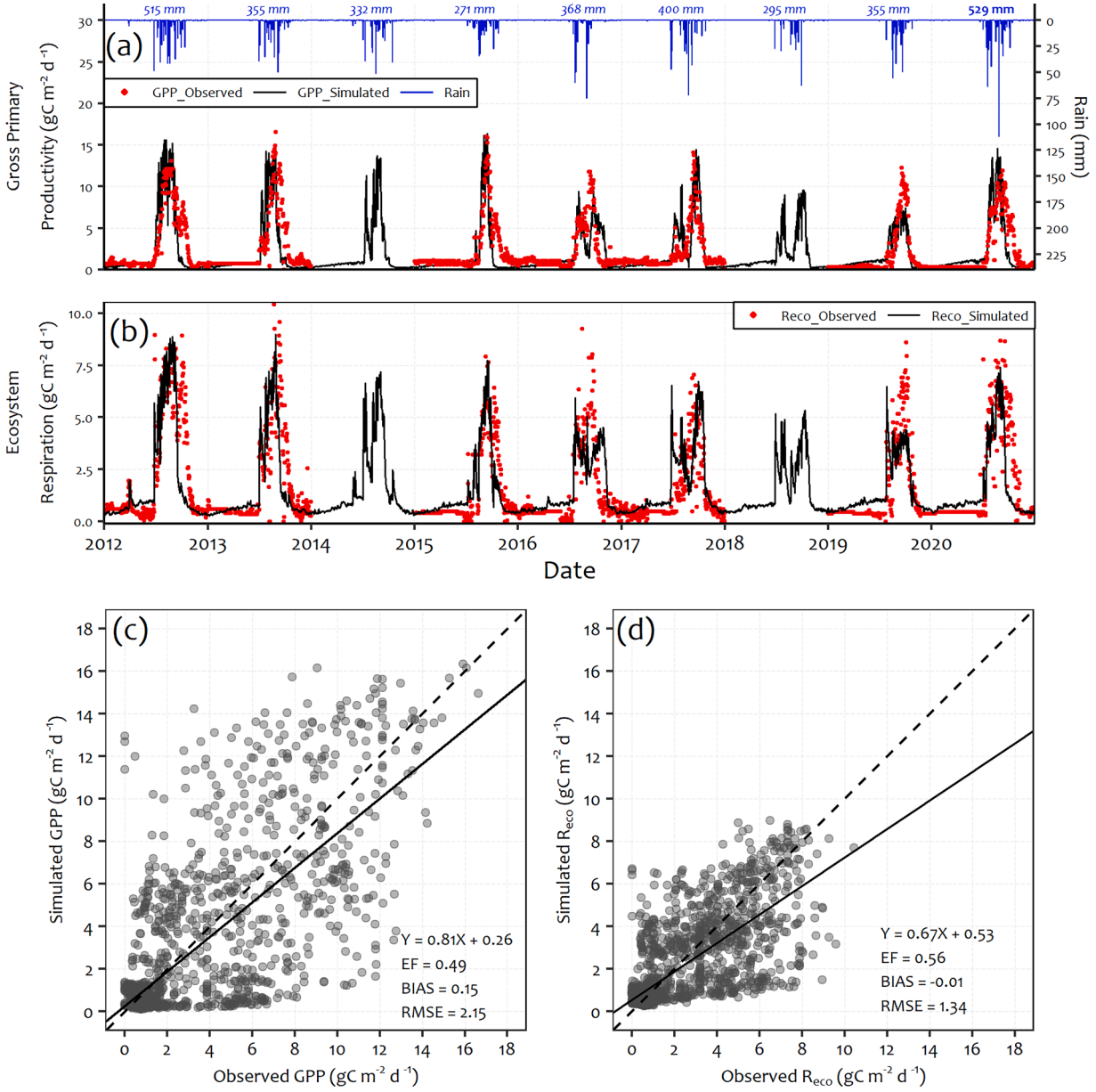

Fig. 3. Time series (2012–2020) of the simulated and observed GPP and R_{eco}. In (a), the blue lines show daily precipitation (mm d^{-1}). The blue numbers at the top of the graph are total annual precipitations. The black line shows the GPP as simulated by STEP-GENDEC-N_2O and DynACof. Red dots indicate the GPP as measured by EC. In (b), the black line is for R_{eco} as simulated by STEP-GENDEC-N_2O and DynACof. Red dots show the R_{eco} as measured by EC. In the scatter plots shown in (c) and (d), the thick black lines are from the respective linear regressions, and the dashed black lines are 1:1 lines. Graph (c) contrasts the values of GPP as simulated by STEP-GENDEC-N_2O and DynACof with the values measured by EC. Graph (d) contrasts the R_{eco} as simulated by STEP-GENDEC-N_2O and DynACof with the R_{eco} values measured by EC. (For interpretation of the references to color in this figure legend, the reader is referred to the web version of this article.)

3.3. CO_2 fluxes: gross primary productivity (GPP) and ecosystem respiration (R_{eco})

The model captured the GPP's seasonal dynamics well, but failed to reproduce the maximum daily GPPs that were observed in 2016 and 2019 (Fig. 3(a)). Despite its difficulties with some daily values (EF = 0.49), the model has a low bias (BIAS = 0.15), and reproduces the overall observed dynamic quite well (Fig. 3(a) and (c)). Simulated R_{eco} values (i.e., the total amounts of CO_2 emitted by vegetation and soil microbes) generally agreed with the observed values, although for some of the years the models did not capture the observed maximum values (Fig. 3(b)). The models explained 56 % of the daily R_{eco} variability, with an RMSE of 1.34 gC m^{-2} d^{-1} and a bias of −0.01 gC m^{-2} d^{-1} (Fig. 3(d)).

Observed annual GPP values ranged from 5.72 to 10.29 tC ha^{-1} yr^{-1} (average: 8.01 ± 1.40 tC ha^{-1} yr^{-1}). Simulated annual GPP values varied from 5.89 to 9.55 tC ha^{-1} yr^{-1} (average: 7.27 ± 1.11 tC ha^{-1} yr^{-1}). The simulated annual GPP is close to the measurements for all years except for 2015, where the value from the simulation is considerably lower than observation (by 2.2 tC ha^{-1} yr^{-1}). Simulated annual R_{eco} values ranged from 5.14 to 7.28 tC ha^{-1} yr^{-1} (average: 5.78 ± 0.6 tC ha^{-1} yr^{-1}), while observed annual R_{eco} values ranged from 4.38 to 8.29 tC ha^{-1} yr^{-1} (average: 5.81 ± 1.33 tC ha^{-1} yr^{-1}). Overall, the simulated annual CO_2 fluxes agreed well with the observations.

Over the course of the study period, the tree layer's simulated daily GPP ranged from 0.09 to 2.11 gC m^{-2} d^{-1}, and the R_{eco} ranged from 0.19 to 0.92 gC m^{-2} d^{-1} (Fig. B.3(c) and (d)). For the same time frame, the herbaceous layer's simulated daily GPP ranged from 0.00 to 13.41 gC m^{-2} d^{-1}, and the R_{eco} ranged from 0 to 8.53 gC m^{-2} d^{-1}. The simulations showed that trees contributed significantly to the annual fluxes (Fig. 4 (b)). Specifically, the tree layer's average annual GPP was 2.68 ± 0.31 tC ha^{-1} yr^{-1} (=37 % of total annual GPP) and its annual average R_{eco} was 1.86 ± 0.17 tC ha^{-1} yr^{-1} (=32 % of total annual R_{eco}). For the herbaceous layer, the average simulated annual GPP was 4.59 ± 1.20 tC ha^{-1} yr^{-1}, and the average simulated annual R_{eco} was 3.91 ± 0.74 tC ha^{-1} yr^{-1}.

3.4. N_2O emissions

The simulations did not capture the observed values in 2013, but the agreement is good for the year 2017. In addition, the observed values are of the same order of magnitude as those from the simulations (Fig. 5(a)). The relationship between the simulation and the observations is weak (EF = −2.03, RMSE of 3.27 ngN m^{-2} s^{-1}). This is primarily attributed to disparities observed during the second campaign of 2013, due to probable spatial heterogeneity not represented by the model, and the limited availability of measurement data points. Additionally, it's important to note that significant emissions events may not have been measured, given the short duration of the measurement campaigns (Fig. 5(b)). The simulation showed that N_2O emission pulses occurred after the first rains. For 2013, the simulation showed an N_2O pulse of 35.69 ngN-N_2O m^{-2} s^{-1} just after the first rain. The simulation showed that this pulse occurred on the same day as the study period's largest daily N_2O emission. The simulation also predicted that the largest daily N_2O fluxes occur during the wet seasons. Moreover, the simulation estimated that the wet season's total N_2O emissions ranged from 65 % of the yearly total in 2018 to 80 % in 2012 (Fig. B.6(a)). Over the course of the study period, the simulated total annual N_2O emissions ranged from 0.25 to 0.46 kgN-N_2O ha^{-1} yr^{-1}, with an annual mean of 0.31 ± 0.06 kgN-N_2O ha^{-1} yr^{-1} for the entire study period (Fig. B.6(a)).

Nitrification was the main process contributing to total N_2O emissions. In 2013, it accounted for 0.24 kgN-N_2O ha^{-1} yr^{-1} (=76 % of the yearly total), and for 0.28 kgN-N_2O ha^{-1} yr^{-1} in 2016 (=92 % of the yearly total). The annual means of N_2O emissions by nitrification and denitrification were 0.27 ± 0.05 and 0.05 ± 0.02 kgN-N_2O ha^{-1} yr^{-1}, respectively (Fig. B.6(b)). Because the WFPS threshold was set to 26 % in the model, denitrification (according the model) occurred only during the wet season, which lasts an average of 100 days per year.

3.5. Impact of livestock manure upon CO_2 and N_2O emissions

To assess the impact of livestock upon CO_2 and N_2O emissions, we ran a modeling scenario with no livestock. That is, the animal load was set to zero, with all other model parameters left unchanged. In this scenario, the decreases in annual CO_2 emissions ranged from 54 % in 2013 (0.73 tC ha^{-1} yr^{-1}) to 80 % in 2019 (1.27 tC ha^{-1} yr^{-1}) (Fig. 6(a)). The decreases in annual N_2O emissions ranged from 76 % in 2013 (0.32 kgN ha^{-1} yr^{-1}) to 93 % in 2018 (0.25 kgN ha^{-1} yr^{-1}) (Fig. 6(b)). These large relative reductions in N_2O emissions are attributable to the notable impact of livestocks upon denitrification processes. The results from this scenario showed that the impact of livestock was relatively greater upon N_2O emissions than upon CO_2 emissions.

3.6. The trees' potential for offsetting emissions

According to the simulation, trees were C sinks throughout the study period, and stored between 0.86 and 2.08 tCO_2eq ha^{-1} yr^{-1} of CO_2 (average = 1.29 ± 0.43 tCO_2eq ha^{-1} yr^{-1}; Fig. 6(c)). Those values, which do not include the exported stems and branches (see the calculation of NEP, Eq. (4)), are consistent with the known range of tree net productivity in the Dahra SPS. (That is, if the net productivity takes into account the amount of CO_2 emitted by trees through respiration, and the amount of C lost through pruning.) The above-mentioned average

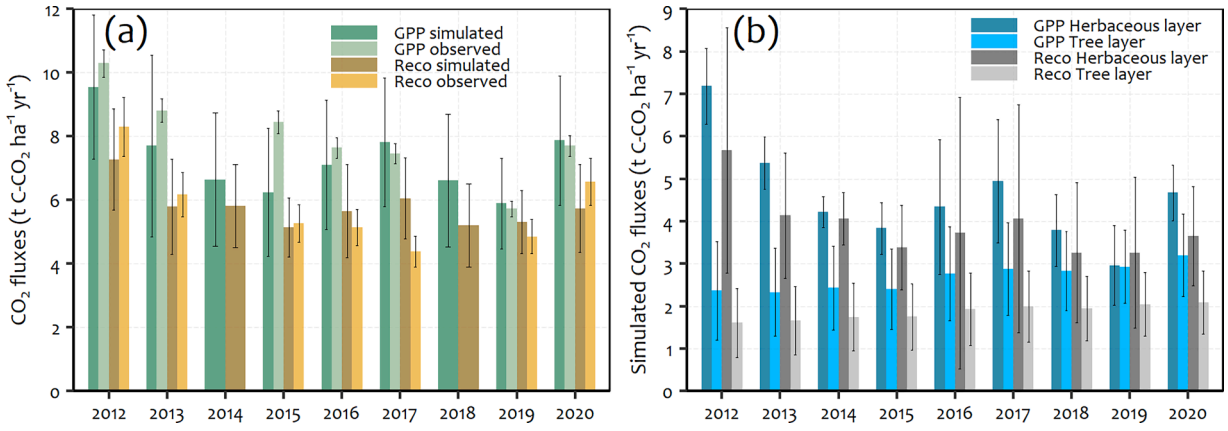

Fig. 4. Time series (2012–2020) of (a) measured and simulated ecosystem GPP and $R_{eco,}$ and (b) partitioning of simulated GPP and R_{eco} by layer, according to the model chain. The herbaceous layer was simulated by STEP-GENDEC-N_2O, and tree layer was simulated by DynACof. Error bars represent the uncertainties of the fluxes (see appendix C).

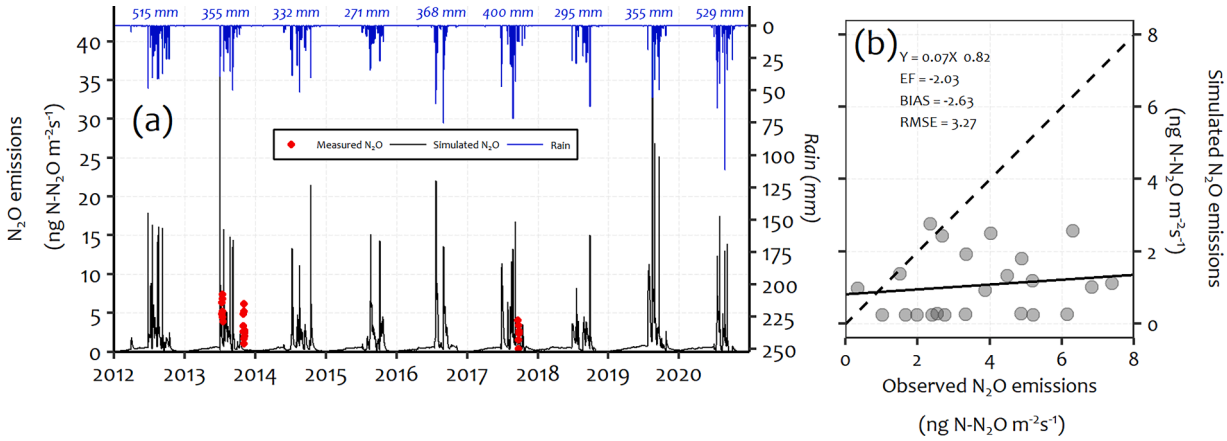

Fig. 5. Time series of soil N_2O emissions (2012–2020). (a) Blue lines show daily precipitation (mm d^{-1}). The blue numbers at the top of the graph are total annual precipitations. Black lines show daily N_2O emissions as simulated by STEP-GENDEC-N_2O. Red dots indicate measured N_2O emissions according to Delon et al. (2017) and Bigaignon et al. (2020). Graph (b) contrasts the values of N_2O emissions as simulated by STEP-GENDEC-N_2O with the values measured. The thick black lines are from the respective linear regressions, and the dashed black lines are 1:1 lines. (For interpretation of the references to color in this figure legend, the reader is referred to the web version of this article.)

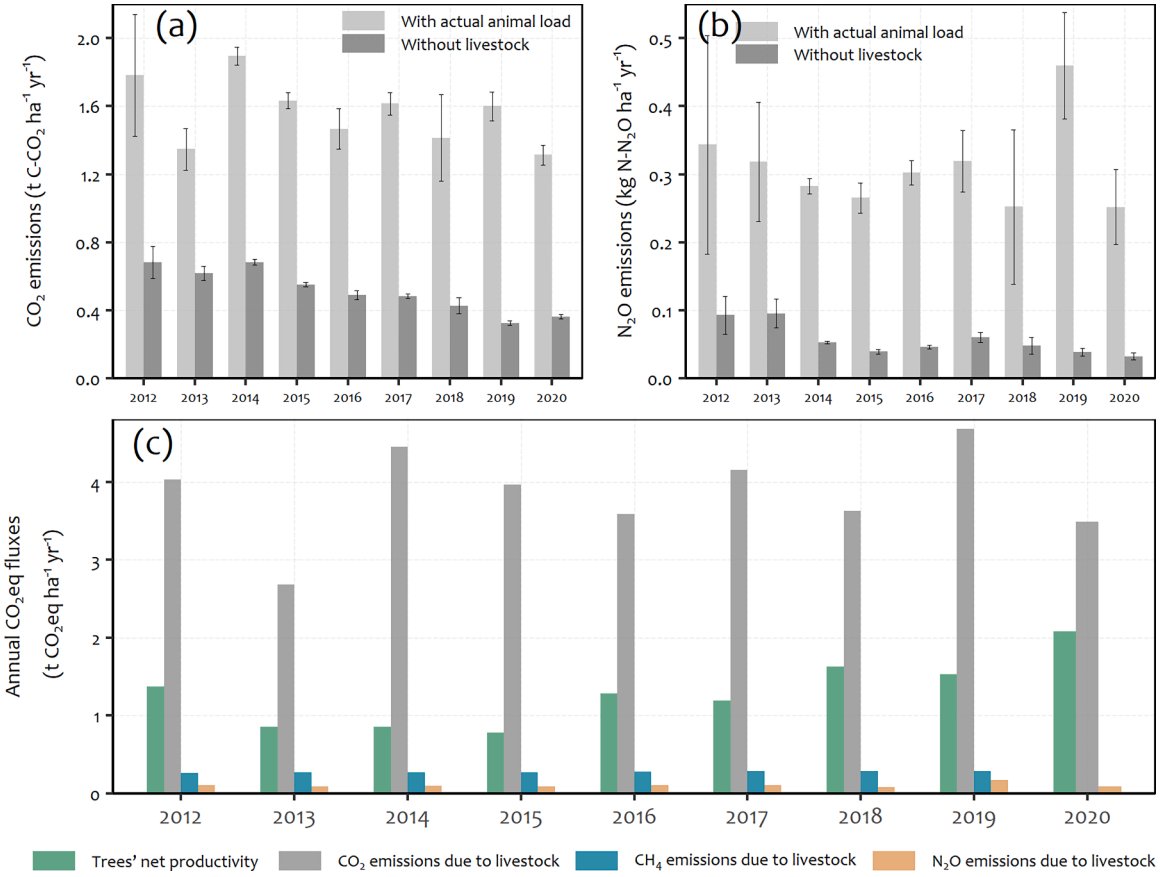

Fig. 6. Time series (2012–2020) of simulated annual emissions of CO_2 and N_2O, with and without livestock. In (a), the bars show the CO_2 emissions from the herbaceous layer with livestock (actual animal load) on the site (light gray bars), and without livestock (dark gray bars). In (b), the bars show simulated annual N_2O emissions with the actual animal load on the site (light gray bars), and without livestock (dark gray bars). Error bars represent the uncertainties associated with the fluxes. The annual CO_2eq fluxes that are indicated by bars in (c) show the trees' potential for offsetting GHG emissions. Green bars are for the trees' net productivity (Eq. (4)); gray bars show the increase in CO_2 emissions due to the presence of livestock; blue bars are for CH_4 emissions from enteric fermentation; and tan bars show the increase in N_2O emissions due to the presence of livestock. In (c), the CO_2 and N_2O emissions due to livestock were simulated with STEP-GENDEC-N_2O. The CH_4 emissions due to livestock (from enteric fermentation) are estimated from the FAO Tier1 dataset. (For interpretation of the references to color in this figure legend, the reader is referred to the web version of this article.)

annual C storage (1.29 ± 0.43 $tCO_2eq\ ha^{-1}\ yr^{-1}$) is an order of magnitude greater than the mean annual increase in N_2O emissions due to livestock at the site (0.10 ± 0.03 $tCO_2eq\ ha^{-1}\ yr^{-1}$). The trees' average annual C storage is also an order of magnitude greater than the site's mean annual CH_4 emissions from enteric fermentation (estimated as 0.28 ± 0.01 $tCO_2eq\ ha^{-1}\ yr^{-1}$ from the FAO Tier1 dataset). A study of these values shows that the trees's average annual C storage exceeds the combined C_{eq} of the livestock-associated N_2O and CH_4 emissions by about 0.9 $tCO_2eq\ ha^{-1}\ yr^{-1}$. Therefore, in the Dahra SPS (with approximately. 81 trees ha^{-1} and an animal load dominated by cattle, goat and sheep), the trees completely offset the CH_4 and N_2O emissions from the livestock. Thus, the trees also store a significant fraction of the increased CO_2 emissions (=3.85 ± 0.59 tCO2eq $ha^{-1}\ yr^{-1}$) from the livestock. More specifically, the trees offset 17.83 % to 40.68 % of the total annual GHG emissions from the livestock at the site (Table A.8).

4. Discussion

4.1. Ability of STEP-GENDEC-N_2O to simulate water fluxes

Overall, the model estimated water fluxes well. This result confirms Grippa et al. (2017) finding that STEP-GENDEC-N_2O performs well in simulating water fluxes of semi-arid ecosystems. STEP-GENDEC-N_2O models the topsoil, which we define as the upper 2 cm of the soil profile, as a shallow layer that is unstable because it is affected by wind and water erosion. This layer determines the resistance to surface evaporation, which itself controls soil evaporation. The processes that produce GHG in the soil take place primarily in the second layer (2–30 cm), and depend heavily upon the availability of water for microbial activity. Therefore, to ensure that the model represents the soil's GHG-production processes realistically, it is important to simulate the water content of this second layer accurately. According to our simulation, the fastest water losses occurred at the end of the 2014 wet season (Fig. 2(a)), and could be due to faster water drainage at that time. The model uses the tipping-bucket approach (Manabe, 1969), in which any excess water within the second soil layer is transferred down to the third layer. Therefore, simulated SWC values of the second layer cannot exceed the field capacity (Delon et al., 2015). This characteristic of the modeling explains why the highest simulated SWC values were approximately 15 % (Fig. 2(a)). The simulated SWC responded rapidly to rainfall events throughout the study period because infiltration is very fast (several decimeters per day) in the study site's sandy soil (sand content >85 %). Consequently, within 2–3 days after a rainfall the rapid infiltration will cause the topsoil's SWC to drop to its previous (dry) value. Because this rapid drying reduces the simulated water availability at the soil surface, the model underestimates soil ET during wet seasons (Fig. 2(b)).

4.2. CO_2 balance of the Dahra SPS

During dry seasons, the observed R_{eco} flux comes largely from trees (Fig. 3) through autotrophic respiration. Indeed, no herbaceous vegetation is present on the site during that season. In addition, the soil is dry, and microbial activity is inhibited. In contrast, during wet seasons the main processes responsible for CO_2 emissions are soil microbial respiration and the autotrophic respiration of herbaceous vegetation.

The annual means of simulated and observed GPP were lower than Tagesson et al.'s (2015) previous observations at the same site, which ranged from 9.35 to 12.63 tC $ha^{-1}\ yr^{-1}$ between 2010 and 2013. For R_{eco}, observations and simulation are comparable to previous observations at Dahra site, which ranged from 6.37 to 8.52 tC $ha^{-1}\ yr^{-1}$ (Tagesson et al., 2015). These CO_2 fluxes at Dahra (i.e., these R_{eco} values) are higher than the published values for other semi-arid sites; e.g., the 3 tC $ha^{-1}\ yr^{-1}$ of R_{eco} observed in Niger by Hanan et al. (1998). This high productivity observed at the Dahra site was attributed to the relatively high concentration of soil nutrients that accrued from animal excreta (Tagesson et al., 2015). Other studies have also highlighted the impact of livestock upon the spatial distribution of soil nutrients in SPS (Manlay et al., 2004; Schlecht et al., 2004). Overall, simulations and observations indicated that the site was a C sink (GPP > R_{eco}) for all years of the study period. However, this result is only apparent, since the eddy-covariance tower does not take the mineralization of exports into account.

4.3. N_2O emissions: specific processes of the Dahra SPS

When SWC approaches or exceeds field capacity, the percentages of soil pore space filled with air or water (WFPS) are better indicators of aerobic and anaerobic microbial activity than water content, or water potential (Aulakh et al., 1992; Miller and Johnson, 1964; Sommers et al., 1981). Analyses carried out on soils in temperate regions found that the theoretical WFPS threshold for denitrification ranges from 40 % (Liu, 1996) to 70 % (Firestone and Davidson, 1989). These thresholds are higher than the maximum WFPS (30 %) observed at Dahra by Bigaignon et al. (2020). At low WFPS levels in semi-arid soils, denitrification may occur either via processes in anaerobic microsites, or via "aerobic denitrification" (Bateman and Baggs, 2005; Carter et al., 1995; Patureau et al., 2000). Indeed, Bateman and Baggs (2005) have shown that aerobic denitrification can occur even at a WFPS as low as 20 %. In a previous study that simulated N_2O emissions at Dahra, Bigaignon et al. (2020) used STEP-GENDEC-N_2O with a WFPS threshold of 9 % well below the 40 % used in the original DNDC module (Liu, 1996). Bigaignon et al. (2020) argued that even at this low WFPS (9 %), denitrification can occur because it is a microbiologically broad process, and the denitrifier community can change with climate, soil, and vegetation type (Li et al., 2019; Meng et al., 2017). However, the value of 9 % WFPS for triggering denitrification processes needed to be re-evaluated in light of the existing literature. In this study, after testing WFPS threshold values ranging from 9 % to 30 %, we chose 26 % because in the simulation, that value triggered N_2O fluxes of the same order of magnitude as the N_2O fluxes that Delon et al. (2017) and Bigaignon et al. (2020) measured at Dahra in 2013 and 2017. Discrepancies between our modeled November 2013 fluxes and the measured ones may be explained by a combination of the measurement's spatial variability and the model's use of plot-scale averages. The dominant contribution of nitrification to the total N_2O emissions from semi-arid soils has been assessed in previous studies (Parton et al., 1996; Wang et al., 1997), but not in African soils (to the authors' knowledge). Our results indicate that denitrification occurs rarely in semi-arid soils with low WFPS, and does not last long, but does emit large amounts of N_2O. However, because denitrification is less frequent, it probably contributes less to the annual N_2O emissions (Fig. B.6(b)). Therefore, nitrification might be the dominant process leading to N_2O emissions in semi-arid soils with low WFPS. Support for this idea is found in the recent work of Zhang et al. (2023), whose high-resolution isotopic analyses revealed that N_2O emissions from the soil of a semi-arid grassland in China originate primarily from nitrification.

In our simulations, the seasonal and interannual dynamics of N_2O emissions were controlled by SWC and (indirectly) by precipitation. N_2O emission peaks occurred after each major rainfall event, especially at the beginnings of wet seasons. This result is in line with previous studies that showed a strong seasonal trend in which N_2O emissions from semi-arid ecosystems peaked at the beginnings of wet seasons (Bigaignon et al., 2020; Brümmer et al., 2008; Jarvis et al., 2007). Our simulated annual mean of N_2O emissions (Fig. B.6(a) and (b): 0.37 ± 0.11 $kgN\text{-}N_2O\ ha^{-1}\ yr^{-1}$) is of the same order of magnitude as the 0.3 to 0.67 $kgN\text{-}N_2O\ ha^{-1}\ yr^{-1}$ range that was estimated in previous studies on African savannas (Bigaignon et al., 2020; Brümmer et al., 2009; Kim et al., 2016). In addition, the CO2eq values of our simulated annual N_2O emissions (0.10 to 0.19 $tCO_2eq\ ha^{-1}\ yr^{-1}$) were comparable to the estimates derived from FAO TIER1 (0.13 to 0.15 tCO2eq $ha^{-1}\ yr^{-1}$) (Fig. B.6(c)).

4.4. Impact of livestock manure upon N_2O emissions

A comparison between the simulations that were run with and without livestock shows that the livestock manure leads to an increase of 76 to 93 % in the total annual N_2O emissions of the Dahra SPS (Fig. 6 (b)). The impacts of livestock upon N budgets and N_2O emissions have been highlighted in previous studies on African sites. For example, Delon et al. (2022) use of rare in-situ measurements in combination with published data showed that the SPS of Dahra has an unbalanced N budget that favors N depletion, and is dominated by the impact of livestock through inputs of N (via manure) and removal of N via grazing. Another study, carried out in Kenya by Butterbach-Bahl et al. (2020), showed that livestock enclosures are an important source of N_2O emissions in African drylands. Livestock affects N_2O emissions through grazing and the related deposition of N via excreta (Dangal et al., 2020). The impact of livestock upon N_2O emissions is actually a result of an increase in soil C, N, and ammonia.

4.5. Trees offset GHG emissions substantially in the Dahra SPS

Using DynACof and STEP-GENDEC-N_2O, we quantified the trees' significant contribution to annual CO_2 fluxes in Dahra (Fig. 4(b)). Even though the daily CO_2 fluxes from the tree layer are smaller than those from the herbaceous layer during wet seasons, the trees end up contributing significantly to the total CO_2 fluxes because they are present in the site throughout the year, while herbaceous vegetation is present only during the wet season (which lasts an average of about 100 days per year). This significant contribution of trees confirms the key role that they play in SPSs. In addition, it is well known that trees have the potential to sequester large amounts of carbon (Mbow et al., 2014). Thus, the presence of livestock within an SPS has a significant impact upon GHG emissions. A great advantage of SPSs over pasture is that the trees can potentially offset the increases in GHG emissions due to livestock. By quantifying this potential, we found that in the Dahra SPS (with approx. 81 trees ha^{-1}), the trees store between 0.86 and 2.08 $tCO_2eq\ ha^{-1}\ yr^{-1}$ of CO_2, thereby offsetting 17.83 to 40.68 % of the increases in GHG emissions that are due to livestock.

4.6. Limitations and uncertainties related to the simulated results

The scarcity of measurement data for the site's N_2O emissions limited the comparisons that could be made between measurements and model outputs. Other limitations may result from both the way in which the model represented the underlying processes of CO_2 and N_2O emissions, and the values of the key parameters that were used. The simulated results could be improved significantly by reducing the uncertainties related to the most sensitive parameters (Fig. Ca & Cb). Additional field studies are needed to improve the representation of key processes like nitrification and denitrification in semi-arid ecosystems. Because the model runs only at a one-day time step, it may smooth pulses in the CO_2 and N_2O fluxes. Although these pulses typically last less than a day (according to observations), they may contribute significantly to annual fluxes (Brumme et al., 1999). Some authors mention the occurrence of fluxes of N_2O from the atmosphere to the soil a phenomenon that may lower the net emissions of GHG (Chapuis-Lardy et al., 2007; Liu et al., 2022; Wen et al., 2017; Xia and Wander, 2022). N_2O uptake may occur at atmospheric pressure when N_2O is slightly soluble at the soil surface, thereby providing N_2O for consumption in subsequent biochemical reactions (Liu et al., 2022). However, to the authors' knowledge no equations are available to simulate such N_2O uptake, which remains low for low WFPS. Nor do equations exist for simulating consumption of N_2O. Because the STEP-GENDEC-N_2O model does not take N_2O uptake into account, the model may overestimate N_2O emissions. However, this possibility is difficult to investigate at present (at least for low values of WFPS) because the literature does not provide any order-of-magnitude estimates of the possible overestimation.

According to our simulations, the livestock have a great impact upon soil heterotrophic respiration (Section 4.4). However, our model did not include enhancement of herbaceous GPP, or the enhancement of autotrophic respiration that results from increased N mineralization of the litter that is trampled into the soil by livestock. (That is, the model does not include any feedback between the additional N that livestock make available to vegetation by trampling, and the increased vegetation that can therefore be trampled into the soil.) The omission of these processes may increase the uncertainties of the C balances and the net CO_2 fluxes from herbaceous mass. Note, too, that the model does not account for carbon exported from the site due to livestock mortality.

We stress here that for at least three reasons, our estimate of the trees' offsetting potential can be considered conservative. First, the grazing pressure in Dahra is four times higher than the average for Sahel (Gilbert et al., 2018). Secondly, the model omits the manure's stimulation of plant productivity. A third reason is that the models do not take the potential capture of N_2O into account. An additional consideration is that STEP-GENDEC-N_2O and DynACof are not coupled: in our study, DynACof simulates the tree layer, exclusively. As a result, the only interaction between the two models is that the tree litter simulated by DynACof feeds the soil's organic-carbon pool in STEP-GENDEC-N_2O. One interaction that is thus overlooked is the effect of the trees' shade upon the herbaceous layer. We assumed that because the tree cover at the Dahra site was sparse, it had little effect (either negative or positive) upon the grass's seasonal above- and below-ground production. This assumption is probably accurate at the whole-site scale, given the low tree density, but the trees may have a localized effect upon grass growth beneath their crowns.

4.7. Impacts

We have shown through this study that a process-based model can be used to realistically quantify the emissions of CO_2 and N_2O from silvopastoral systems over several years. This time scale can hardly be covered by field measurements. Therefore, the process-base model can fulfil the valuable function of providing important long-term statistics on the carbon and nitrogen footprints of Sahelian silvopastoral systems. We showed through this modeling exercise that livestock have a significant impact upon the ecosystems' CO_2 and N_2O emissions. However, the impact is reduced in silvopastoral systems thanks to the presence of trees that sequester carbon.

The overall role of livestock in the input and sequestration of carbon (including methane) needs to be assessed more intensively, with the goal of providing an objective assessment of GHG emissions from SPSs in general. To reduce CO_2 and N_2O emissions in Sahelian silvopastoral systems, policy makers should develop concrete livestock-management policies that are adapted to the Sahel. Some initiatives of this sort are underway, and Senegal is already aiming at promoting sustainable land-management technologies, such as agroforestry (Ministère de l'Environnement, du Développement durable et de la Transition écologique du Sénégal, 2015). Among the lines of thought to consider are increasing the density of tree cover, improving tree management, offering alternatives to wood energy, and controlling the seasonal movements of livestock. At present, implementation of mitigation strategies in the Sahel is very challenging because of incomplete inventories of the three main GHGs (CO_2, N_2O, and CH_4), and insufficient data on the populations and movement of livestock. Therefore, in order to implement mitigation policies and participate in reducing the rate of climate change, Sahelian countries need institutional structure, investments, and reliable data on GHG emissions from different ecosystems (e.g., livestock systems, silvopastoral systems, and agro-silvopastoral systems).

5. Conclusions

Our study demonstrated that process-based models can successfully

simulate CO_2 and N_2O emissions at the ecosystem scale, thus providing insights into the possible long-term biophysical control of those emissions. Simulations indicated that nitrification is the dominant process leading to N_2O emissions in semi-arid soils with low WFPS. We showed that in a silvopastoral system with approximately 81 trees ha^{-1}, and an animal load dominated by cattle, goats, and sheep, the trees offset 18 % to 41 % of the increases in total GHG emissions from the livestock. The modeling approach developed in this work can be useful for informing policies for climate-change adaptation and mitigation in Sahelian SPSs. However, more field data on GHG emissions, livestock populations, and livestock movements are needed to develop a full picture of the carbon footprint of Sahelian SPSs.

Code availability

The STEP-GENDEC-N_2O model can be found at https://zenodo.org/record/7973200. The DynACof model is available at https://doi.org/10.5281/zenodo.1256816.

Mention

This document has been produced with the assistance of the European Union. Its content is the sole responsibility of the authors, and should not be taken as reflecting any position of the European Union.

Funding

This work was supported by the “Carbon sequestration and greenhouse gas emissions in (agro) silvopastoral ecosystems in the Sahelian CILSS states” (CaSSECS) project (FOOD/2019/410-169), which was itself supported by European Union under the “Development of Smart Innovation through Research in Agriculture” (DeSIRA) Initiative; and The European Union’s Horizon 2020 research and innovation programme under the Marie Skłodowska-Curie grant agreement (871944). Additional funding for TT was provided by FORMAS (Dnr. 2021-00644) and the Swedish National Space Agency (SNSA 2021-00144 and 2021-00111).

CRediT authorship contribution statement

Yélognissè Agbohessou: Conceptualization, Methodology, Writing – original draft, Writing – review & editing. **Claire Delon:** Conceptualization, Methodology, Writing – original draft, Writing – review & editing. **Eric Mougin:** Conceptualization, Methodology, Writing – original draft, Writing – review & editing. **Manuela Grippa:** Conceptualization, Methodology, Writing – original draft, Writing – review & editing. **Torbern Tagesson:** Conceptualization, Methodology, Writing – original draft, Writing – review & editing. **Moussa Diedhiou:** Writing – review & editing. **Seydina Ba:** Writing – review & editing. **Daouda Ngom:** Writing – review & editing. **Rémi Vezy:** Writing – review & editing. **Ousmane Ndiaye:** Writing – review & editing. **Mohamed H. Assouma:** Writing – review & editing. **Mamadou Diawara:** Writing – review & editing. **Olivier Roupsard:** Conceptualization, Methodology, Writing – original draft, Writing – review & editing.

Declaration of Competing Interest

The authors declare that they have no known competing financial interests or personal relationships that could have appeared to influence the work reported in this paper.

Data availability

Data will be made available on request.

Acknowledgments

The authors thank AMMA-CATCH for funding the collection and analysis of in-situ soil samples; Cofélas Fassinou for sharing his vegetation data; and M. Dendoncker and C. Vincke for sharing relevant literature on allometric equations. We thank D.L. Moorhead for providing us with the GENDEC model. We acknowledge the NASA Langley Research Center’s POWER Project (funded through the NASA Earth Science Directorate Applied Science Program) for the use of the POWER NASA climate products. The «Laboratoire des Moyens Analytiques» (UAR IMAGO—LAMA certified ISO9001:2015), at IRD («Institut de Recherche pour le Dévelopement») analyzed the soil samples in Dakar (http://www.imago.ird.fr/moyens-analytiques/dakar). We thank Dr. James Smith for revising the English.

Supplementary materials

Supplementary material associated with this article can be found, in the online version, at doi:10.1016/j.agrformet.2023.109780.

References

Assouma, M.H., Serça, D., Guérin, F., Blanfort, V., Lecomte, P., Touré, I., Ickowicz, A., Manlay, R.J., Bernoux, M., Vayssières, J., 2017. Livestock induces strong spatial heterogeneity of soil CO_2, N_2O and CH_4 emissions within a semi-arid sylvo-pastoral landscape in West Africa. J. Arid Land 9, 210–221. https://doi.org/10.1007/s40333-017-0001-y.

Aulakh, M.S., Doran, J.W., Mosier, A.R., 1992. Soil denitrification—Significance, measurement, and effects of management. Advances in Soil Science. Springer, pp. 1–57.

Aulakh, M.S., Doran, J.W., Walters, D.T., Power, J.F., 1991. Legume residue and soil water effects on denitrification in soils of different textures. Soil Biol. Biochem. 23, 1161–1167.

Bajracharya, R.M., Lal, R., Kimble, J.M., 2000. Diurnal and seasonal CO_2–C flux from soil as related to erosion phases in central Ohio. Soil Sci. Soc. Am. J. 64, 286–293.

Bateman, E.J., Baggs, E.M., 2005. Contributions of nitrification and denitrification to N_2O emissions from soils at different water-filled pore space. Biol. Fertil. Soils 41, 379–388. https://doi.org/10.1007/s00374-005-0858-3.

Bentzon-Tarp, A., Helgadóttir, D., Van den Meersche, K., Gay, F., Priemé, A., Roupsard, O., Mages, C., Elberling, B., 2023. Spatial-temporal variations of nitrous oxide emissions in coffee agroforestry systems in Costa Rica. Agric. Ecosyst. Environ. 343, 108257.

Bigaignon, L., Delon, C., Ndiaye, O., Galy-Lacaux, C., Serça, D., Guérin, F., Tallec, T., Merbold, L., Tagesson, T., Fensholt, R., André, S., Galliau, S., 2020. Understanding N_2O emissions in African ecosystems: assessments from a semi-arid Savanna Grassland in Senegal and sub-tropical agricultural fields in Kenya 26.

Brumme, R., Borken, W., Finke, S., 1999. Hierarchical control on nitrous oxide emission in forest ecosystems. Glob. Biogeochem. Cycles 13, 1137–1148.

Brümmer, C., Falk, U., Papen, H., Szarzynski, J., Wassmann, R., Brüggemann, N., 2008. Diurnal, seasonal, and interannual variation in carbon dioxide and energy exchange in shrub savanna in Burkina Faso (West Africa). J. Geophys. Res. Biogeosci. 113 https://doi.org/10.1029/2007JG000583.

Brümmer, C., Papen, H., Wassmann, R., Brüggemann, N., 2009. Termite mounds as hot spots of nitrous oxide emissions in South-Sudanian savanna of Burkina Faso (West Africa). Geophys. Res. Lett. 36, L09814. https://doi.org/10.1029/2009GL037351.

Butterbach-Bahl, K., Gettel, G., Kiese, R., Fuchs, K., Werner, C., Rahimi, J., Barthel, M., Merbold, L., 2020. Livestock enclosures in drylands of Sub-Saharan Africa are overlooked hotspots of N_2O emissions. Nat. Commun. 11, 4644. https://doi.org/10.1038/s41467-020-18359-y.

Carter, J.P., Hsaio, Y.H., Spiro, S., Richardson, D.J., 1995. Soil and sediment bacteria capable of aerobic nitrate respiration. Appl. Environ. Microbiol. 61, 2852–2858.

Chapman, M., Walker, W.S., Cook-Patton, S.C., Ellis, P.W., Farina, M., Griscom, B.W., Baccini, A., 2020. Large climate mitigation potential from adding trees to agricultural lands. Glob. Change Biol. 26, 4357–4365. https://doi.org/10.1111/gcb.15121.

Chapuis-Lardy, L., Wrage, N., Metay, A., Chotte, J.-L., Bernoux, M., 2007. Soils, a sink for N_2O? A review. Glob. Change Biol. 13, 1–17. https://doi.org/10.1111/j.1365-2486.2006.01280.x.

Cissé, M.I., 1980. The browse production of some trees of the Sahel: relationships between maximum foliage biomass and various physical parameters. In: Browse in Africa, International Symposium on Browse in Africa. Addis Abab, Ethiopia, pp. 205–210. https://books.google.sn/books?id=f8wzMTZzPZYC&printsec=frontcover&hl=fr#v=onepage&q&f=false.

Dangal, S.R.S., Tian, H., Pan, S., Zhang, L., Xu, R., 2020. Greenhouse gas balance in global pasturelands and rangelands. Environ. Res. Lett. 15, 104006 https://doi.org/10.1088/1748-9326/abaa79.

Davidson, E.A., Verchot, L.V., 2000. Testing the hole-in-the-pipe model of nitric and nitrous oxide emissions from soils using the TRAGNET database. Glob. Biogeochem. Cycles 14, 1035–1043.

Delon, C., Galy-Lacaux, C., Barret, B., Ndiaye, O., Serça, D., Guérin, F., Gardrat, E., Mougin, E., Agbohessou, Y.F., Probst, A., 2022. Nitrogen budget and critical load determination at a Sahelian grazed grassland site. Nutr. Cycl. Agroecosyst. https://doi.org/10.1007/s10705-022-10220-6.

Delon, C., Galy-Lacaux, C., Serça, D., Loubet, B., Camara, N., Gardrat, E., Saneh, I., Fensholt, R., Tagesson, T., Le Dantec, V., Sambou, B., Diop, C., Mougin, E., 2017. Soil and vegetation-atmosphere exchange of NO, NH_3, and N_2O from field measurements in a semi arid grazed ecosystem in Senegal. Atmos. Environ. 156, 36–51. https://doi.org/10.1016/j.atmosenv.2017.02.024.

Delon, C., Galy-Lacaux, C., Serça, D., Personne, E., Mougin, E., Adon, M., Le Dantec, V., Loubet, B., Fensholt, R., Tagesson, T., 2019. Modelling land–atmosphere daily exchanges of NO, NH3, and CO2 in a semi-arid grazed ecosystem in Senegal. Biogeosciences 16, 2049–2077. https://doi.org/10.5194/bg-16-2049-2019.

Delon, C., Mougin, E., Serça, D., Grippa, M., Hiernaux, P., Diawara, M., Galy-Lacaux, C., Kergoat, L., 2015. Modelling the effect of soil moisture and organic matter degradation on biogenic NO emissions from soils in Sahel rangeland (Mali). Biogeosciences 12, 3253–3272. https://doi.org/10.5194/bg-12-3253-2015.

Elberling, B., Fensholt, R., Larsen, L., Petersen, A.S., Sandholt, I., 2003a. Water content and land use history controlling soil CO_2 respiration and carbon stock in savanna soil and groundnut fields in semi-arid Senegal. Geogr. Tidsskr. - Danish J. Geogr. 103, 47–56.

Elberling, B., Touré, A., Rasmussen, K., 2003b. Changes in soil organic matter following groundnut–millet cropping at three locations in semi-arid Senegal, West Africa. Agric., Ecosyst. Environ. 96, 37–47.

FAOSTAT, 2022. FAOSTAT database collections. Food and Agriculture Organization of the United Nations. [WWW Document]. URL https://www.fao.org/faostat/en/#data/GT (accessed 8.22.22).

Fensholt, R., Sandholt, I., 2005. Evaluation of MODIS and NOAA AVHRR vegetation indices with in situ measurements in a semi-arid environment. Int. J. Remote Sens. 26, 2561–2594.

Fensholt, R., Sandholt, I., Stisen, S., 2006. Evaluating MODIS, MERIS, and VEGETATION vegetation indices using in situ measurements in a semiarid environment. IEEE Trans. Geosci. Remote Sens. 44, 1774–1786.

Firestone, M.K., Davidson, E.A., 1989. Microbiological basis of NO and N_2O production and consumption in soil. Exchange of Trace Gases between Terrestrial Ecosystems and the Atmosphere. Wiley, New York, NY, pp. 7–21.

Gilbert, M., Nicolas, G., Cinardi, G., Van Boeckel, T.P., Vanwambeke, S.O., Wint, G.R.W., Robinson, T.P., 2018. Global distribution data for cattle, buffaloes, horses, sheep, goats, pigs, chickens and ducks in 2010. Sci. Data 5, 180227. https://doi.org/10.1038/sdata.2018.227.

Godde, C.M., Boone, R.B., Ash, A.J., Waha, K., Sloat, L.L., Thornton, P.K., Herrero, M., 2020. Global rangeland production systems and livelihoods at threat under climate change and variability. Environ. Res. Lett. 15, 044021 https://doi.org/10.1088/1748-9326/ab7395.

Grippa, M., Kergoat, L., Boone, A., Peugeot, C., Demarty, J., Cappelaere, B., Gal, L., Hiernaux, P., Mougin, E., Ducharne, A., Dutra, E., Anderson, M., Hain, C., ALMIP2 Working Group, 2017. Modeling surface runoff and water fluxes over contrasted soils in the pastoral sahel: evaluation of the ALMIP2 land surface models over the Gourma Region in Mali. J. Hydrometeorol. 18, 1847–1866. https://doi.org/10.1175/JHM-D-16-0170.1.

Hanan, N.P., Kabat, P., Dolman, A.J., Elbers, J.A., 1998. Photosynthesis and carbon balance of a Sahelian fallow savanna. Glob. Change Biol. 4, 523–538.

Hiernaux, P., Adamou Kalilou, A., Kergoat, L., Brandt, M., Mougin, E., Fitts, Y., 2022. Woody plant decline in the Sahel of western Niger (1996–2017): is it driven by climate or land use changes? J. Arid Environ. 200, 104719 https://doi.org/10.1016/j.jaridenv.2022.104719.

IPCC, 2022. Climate Change 2022: impacts, Adaptation, and Vulnerability. Contribution of Working Group II to the Sixth Assessment Report of the Intergovernmental Panel on Climate Change [H.-O. Pörtner, D.C. Roberts, M. Tignor, E.S. Poloczanska, K. Mintenbeck, A. Alegría, M. Craig, S. Langsdorf, S. Löschke, V. Möller, A. Okem, B. Rama (eds.)]. 3056. doi:10.1017/9781009325844.

IPCC, 2014. Climate Change 2014: synthesis Report. Contribution of Working Groups I, II and III to the Fifth Assessment Report of the Intergovernmental Panel on Climate Change [Core Writing Team, R.K. Pachauri and L.A. Meyer (eds.)]. 151.

IPCC, 2006. 2006 IPCC Guidelines for National Greenhouse Gas Inventories.

Jarvis, P., Rey, A., Petsikos, C., Wingate, L., Rayment, M., Pereira, J., Banza, J., David, J., Miglietta, F., Borghetti, M., 2007. Drying and wetting of Mediterranean soils stimulates decomposition and carbon dioxide emission: the "Birch effect''. Tree Physiol. 27, 929–940.

Kim, D.-G., Thomas, A.D., Pelster, D., Rosenstock, T.S., Sanz-Cobena, A., 2016. Greenhouse gas emissions from natural ecosystems and agricultural lands insub-Saharan Africa: synthesis of available data and suggestions for furtherresearch. Biogeosciences 13, 4789–4809. https://doi.org/10.5194/bg-13-4789-2016.

Knowles, R., 1982. Denitrification. Microbiol. Rev. 46, 28.

Latham, J., Cumani, R., Rosati, I., Bloise, M., 2014. Global Land Cover Share (GLC-SHARE) Database Beta-Release Version 1.0-2014, 29. FAO, Rome, Italy.

Li, C., 2007. Quantifying greenhouse gas emissions from soils: scientific basis and modeling approach. Soil Sci. Plant Nutr. 53, 344–352. https://doi.org/10.1111/j.1747-0765.2007.00133.x.

Li, C.S., 2000. Modeling trace gas emissions from agricultural ecosystems. In: Wassmann, R., Lantin, R.S., Neue, H.-U. (Eds.), Methane Emissions from Major Rice Ecosystems in Asia. Springer, Netherlands, Dordrecht, pp. 259–276. https://doi.org/10.1007/978-94-010-0898-3_20.

Li, H., Zhang, Y., Wang, T., Feng, S., Ren, Q., Cui, Z., Cao, C., 2019. Responses of soil denitrifying bacterial communities carrying nirS, nirK, and nosZ genes to revegetation of moving sand dunes. Ecol. Indic. 107, 105541.

Liu, Y., 1996. Modeling the Emissions of Nitrous Oxide (N_2O) and Methane (CH_4) from the Terrestrial Biosphere to the Atmosphere. Massachusetts Institute of Technology.

Liu, Y., Wu, X., Wu, T., Zhao, L., Li, R., Li, W., Hu, G., Zou, D., Ni, J., Du, Y., Wang, M., Li, Z., Wei, X., Yan, X., 2022. Soil texture and its relationship with environmental factors on the Qinghai–Tibet Plateau. Remote Sens. 14, 3797. https://doi.org/10.3390/rs14153797.

Manabe, S., 1969. Climate and the ocean circulation: I. The atmospheric circulation and the hydrology of the earth's surface. Mon. Weather Rev. 97, 739–774.

Manlay, R.J., Ickowicz, A., Masse, D., Feller, C., Richard, D., 2004. Spatial carbon, nitrogen and phosphorus budget in a village of the West African savanna—II. Element flows and functioning of a mixed-farming system. Agric. Syst. 79, 83–107.

Mbow, C., Fensholt, R., Rasmussen, K., Diop, D., 2013. Can vegetation productivity be derived from greenness in a semi-arid environment? Evidence from ground-based measurements. J. Arid Environ. 97, 56–65.

Mbow, C., Van Noordwijk, M., Luedeling, E., Neufeldt, H., Minang, P.A., Kowero, G., 2014. Agroforestry solutions to address food security and climate change challenges in Africa. Curr. Opin. Environ. Sustain. 6, 61–67.

Meng, H., Wu, R., Wang, Y.-F., Gu, J.-D., 2017. A comparison of denitrifying bacterial community structures and abundance in acidic soils between natural forest and re-vegetated forest of Nanling nature reserve in southern China. J. Environ. Manag. 198, 41–49.

Miller, R.D., Johnson, D.D., 1964. The effect of soil moisture tension on carbon dioxide evolution, nitrification, and nitrogen mineralization. Soil Sci. Soc. Am. J. 28, 644–647.

Ministère de l'Environnement, du Développement durable et de la Transition écologique du Sénégal, 2015. Contribution prévue déterminée au niveau national (CPDN).

Montagnini, F., Ibrahim, M., Murgueitio, E., 2013. Silvopastoral systems and climate change mitigation in Latin America. Bois Forêts Trop. 316, 3–16.

Monteith, J.L., 1965. Evaporation and environment. In: GE Fogg Symposium of the Society for Experimental Biology. The State and Movement of Water in Living Organisms 19, pp. 205–234.

Moorhead, D.L., Reynolds, J.F., 1991. A general model of litter decomposition in the northern Chihuahuan Desert. Ecol. Model. 56, 197–219. https://doi.org/10.1016/0304-3800(91)90200-K.

Mougin, E., Demarez, V., Diawara, M., Hiernaux, P., Soumaguel, N., Berg, A., 2014. Estimation of LAI, fAPAR and fCover of Sahel rangelands (Gourma, Mali). Agric. For. Meteorol. 198–199, 155–167. https://doi.org/10.1016/j.agrformet.2014.08.006.

Mougin, E., Lo Seena, D., Rambal, S., Gaston, A., Hiernaux, P., 1995. A regional Sahelian grassland model to be coupled with multispectral satellite data. I: model description and validation. Remote Sens. Environ. 52, 181–193. https://doi.org/10.1016/0034-4257(94)00126-8.

Newbold, T., Hudson, L.N., Hill, S.L.L., Contu, S., Lysenko, I., Senior, R.A., Börger, L., Bennett, D.J., Choimes, A., Collen, B., Day, J., De Palma, A., Díaz, S., Echeverria-Londoño, S., Edgar, M.J., Feldman, A., Garon, M., Harrison, M.L.K., Alhusseini, T., Ingram, D.J., Itescu, Y., Kattge, J., Kemp, V., Kirkpatrick, L., Kleyer, M., Correia, D.L. P., Martin, C.D., Meiri, S., Novosolov, M., Pan, Y., Phillips, H.R.P., Purves, D.W., Robinson, A., Simpson, J., Tuck, S.L., Weiher, E., White, H.J., Ewers, R.M., Mace, G. M., Scharlemann, J.P.W., Purvis, A., 2015. Global effects of land use on local terrestrial biodiversity. Nature 520, 45–50. https://doi.org/10.1038/nature14324.

Ojeda, J.J., Volenec, J.J., Brouder, S.M., Caviglia, O.P., Agnusdei, M.G., 2017. Evaluation of agricultural production systems simulator as yield predictor of *Panicum virgatum* and *Miscanthus* × *giganteus* in several US environments. GCB Bioenergy 9, 796–816.

Parmesan, C., Morecroft, M., Trisurat, Y., Adrian, R., Anshari, G., Arneth, A., Gao, Q., Gonzalez, P., Harris, R., Price, J., Stevens, N., Talukdarr, G., Strutz, S., Ackerly, D., Anderson, E., Boyd, P., Birkmann, J., Bremerich, V., Brotons, L., Young, K., 2022. IPCC AR6 WGII Chapter 2—Terrestrial and freshwater ecosystems and their services. In: Pörtner, H.-O., Roberts, D.C., Tignor, M., Poloczanska, E.S., Mintenbeck, K., Alegría, A., Craig, M., Langsdorf, S., Löschke, S., Möller, V., Okem, A., Rama, B. (Eds.), Climate Change 2022: Impacts, Adaptation, and Vulnerability. Contribution of Working Group II to the Sixth Assessment Report of the Intergovernmental Panel on Climate Change. Cambridge, UK and New York, NY, USA, pp. 197–377. https://doi.org/10.1017/9781009325844.004.

Parton, W.J., Mosier, A.R., Ojima, D.S., Valentine, D.W., Schimel, D.S., Weier, K., Kulmala, A.E., 1996. Generalized model for N_2 and N_2O production from nitrification and denitrification. Glob. Biogeochem. Cycles 10, 401–412.

Patureau, D., Zumstein, E., Delgenès, J.-P., Moletta, R., 2000. Aerobic denitrifiers isolated from diverse natural and managed ecosystems. Microb. Ecol. 39, 145–152.

Pörtner, H.-O., Roberts, D.C., Adams, H., Adler, C., Aldunce, P., Ali, E., Begum, R.A., Betts, R., Kerr, R.B., Biesbroek, R., 2022. Climate change 2022: impacts, adaptation and vulnerability. IPCC Sixth Assessment Report.

Poupon, H., 1980. Structure et dynamique de la strate ligneuse d'une steppe sahélienne au nord du Sénégal. IRD Editions.

Reth, S., Reichstein, M., Falge, E., 2005. The effect of soil water content, soil temperature, soil pH-value and the root mass on soil CO_2 efflux—A modified model. Plant Soil 268, 21–33. https://doi.org/10.1007/s11104-005-0175-5.

Robertson, G.P., Paul, E.A., 2000. Decomposition and soil organic matter dynamics. Methods in Ecosystem Science. Springer, pp. 104–116.

Savary, S., Nelson, A., Willocquet, L., Pangga, I., Aunario, J., 2012. Modeling and mapping potential epidemics of rice diseases globally. Crop. Prot. 34, 6–17.

Schlecht, E., Hiernaux, P., Achard, F., Turner, M.D., 2004. Livestock related nutrient budgets within village territories in western Niger. Nutr. Cycl. Agroecosyst. 68, 199–211.

Sobol, I.M., 2001. Global sensitivity indices for nonlinear mathematical models and their Monte Carlo estimates. Math. Comput. Simul. 55, 271–280.

Sommers, L.E., Gilmour, C.M., Wildung, R.E., Beck, S.M., 1981. The effect of water potential on decomposition processes in soils. Water Potential Relat. Soil Microbiol. 9, 97–117.

Stackhouse Jr., P.W., Zhang, T., Westberg, D., Barnett, A.J., Bristow, T., Macpherson, B., Hoell, J.M., Hamilton, B.A., 2018. POWER Release 8.0. 1 (with GIS Applications) Methodtology (Data Parameters, Sources, & Validation). Documentation Date December, 12, 2018.

Stewart, B.A., Porter, L.K., Clark, F.E., 1963. The reliability of a micro-Dumas procedure for determining total nitrogen in soil. Soil. Sci. Soc. Am. J. 27, 377–380.

Tagesson, T., Ardö, J., Guiro, I., Cropley, F., Mbow, C., Horion, S., Ehammer, A., Mougin, E., Delon, C., Galy-Lacaux, C., Fensholt, R., 2016a. Very high CO_2 exchange fluxes at the peak of the rainy season in a West African grazed semi-arid savanna ecosystem. Geogr. Tidsskr. - Danish J. Geogr. 116, 93–109. https://doi.org/10.1080/00167223.2016.1178072.

Tagesson, T., Fensholt, R., Cappelaere, B., Mougin, E., Horion, S., Kergoat, L., Nieto, H., Mbow, C., Ehammer, A., Demarty, J., Ardö, J., 2016b. Spatiotemporal variability in carbon exchange fluxes across the Sahel. Agric. For. Meteorol. 226–227, 108–118. https://doi.org/10.1016/j.agrformet.2016.05.013.

Tagesson, T., Fensholt, R., Cropley, F., Guiro, I., Horion, S., Ehammer, A., Ardö, J., 2015. Dynamics in carbon exchange fluxes for a grazed semi-arid savanna ecosystem in West Africa. Agric. Ecosyst. Environ. 205, 15–24. https://doi.org/10.1016/j.agee.2015.02.017.

Tian, H., Chen, G., Lu, C., Xu, X., Ren, W., Zhang, B., Banger, K., Tao, B., Pan, S., Liu, M., Zhang, C., Bruhwiler, L., Wofsy, S., 2015. Global methane and nitrous oxide emissions from terrestrial ecosystems due to multiple environmental changes. Ecosyst. Health Sustain. 1, 1–20. https://doi.org/10.1890/EHS14-0015.1.

Tian, H., Xu, R., Canadell, J.G., Thompson, R.L., Winiwarter, W., Suntharalingam, P., Davidson, E.A., Ciais, P., Jackson, R.B., Janssens-Maenhout, G., Prather, M.J., Regnier, P., Pan, N., Pan, S., Peters, G.P., Shi, H., Tubiello, F.N., Zaehle, S., Zhou, F., Arneth, A., Battaglia, G., Berthet, S., Bopp, L., Bouwman, A.F., Buitenhuis, E.T., Chang, J., Chipperfield, M.P., Dangal, S.R.S., Dlugokencky, E., Elkins, J.W., Eyre, B. D., Fu, B., Hall, B., Ito, A., Joos, F., Krummel, P.B., Landolfi, A., Laruelle, G.G., Lauerwald, R., Li, W., Lienert, S., Maavara, T., MacLeod, M., Millet, D.B., Olin, S., Patra, P.K., Prinn, R.G., Raymond, P.A., Ruiz, D.J., van der Werf, G.R., Vuichard, N., Wang, J., Weiss, R.F., Wells, K.C., Wilson, C., Yang, J., Yao, Y., 2020. A comprehensive quantification of global nitrous oxide sources and sinks. Nature 586, 248–256. https://doi.org/10.1038/s41586-020-2780-0.

Torres, C.M.M.E., Jacovine, L.A.G., Nolasco de Olivera Neto, S., Fraisse, C.W., Soares, C. P.B., de Castro Neto, F., Ferreira, L.R., Zanuncio, J.C., Lemes, P.G., 2017. Greenhouse gas emissions and carbon sequestration by agroforestry systems in southeastern Brazil. Sci. Rep. 7, 16738. https://doi.org/10.1038/s41598-017-16821-4.

Trisos, C.H., Adelekan, I.O., Totin, E., Ayanlade, A., Efitre, J., Gemeda, A., Kalaba, K., Lennard, C., Masao, C., Mgaya, Y., Ngaruiya, G., Olago, D., Simpson, N.P., Zakieldeen, S., 2022. Africa. In: Pörtner, H.-O., Roberts, D.C., Tignor, M., Poloczanska, E.S., Mintenbeck, K., Alegría, A., Craig, M., Langsdorf, S., Löschke, S., Möller, V., Okem, A., Rama, B. (Eds.), Climate Change 2022: Impacts, Adaptation and Vulnerability. Contribution of Working Group II to the Sixth Assessment Report of the Intergovernmental Panel on Climate Change. Cambridge University Press.

Van Wart, J., Grassini, P., Yang, H., Claessens, L., Jarvis, A., Cassman, K.G., 2015. Creating long-term weather data from thin air for crop simulation modeling. Agric. For. Meteorol. 209, 49–58.

Vezy, R., Buis, S., Lecharpentier, P., Giner, M., 2021. CroPlotR: a package to analyse crop model simulations outputs with plots and statistics. doi:10.5281/zenodo.7019749.

Vezy, R., le Maire, G., Christina, M., Georgiou, S., Imbach, P., Hidalgo, H.G., Alfaro, E.J., Blitz-Frayret, C., Charbonnier, F., Lehner, P., Loustau, D., Roupsard, O., 2020. DynACof: a process-based model to study growth, yield and ecosystem services of coffee agroforestry systems. Environ. Model. Softw. 124, 104609 https://doi.org/10.1016/j.envsoft.2019.104609.

Walkey, A., Black, I.A., 1934. Determination of organic carbon in soil. Soil Sci. 37, 29–38.

Wang, Y.-P., Meyer, C.P., Galbally, I.E., Smith, C.J., 1997. Comparisons of field measurements of carbon dioxide and nitrous oxide fluxes with model simulations for a legume pasture in southeast Australia. J. Geophys. Res. 102, 28013–28024. https://doi.org/10.1029/97JD02063.

Ward, B.B., 2013. Nitrification. Encyclopedia of Ecology. Elsevier, pp. 351–358. https://doi.org/10.1016/B978-0-12-409548-9.00697-7.

Wen, Y., Corre, M.D., Schrell, W., Veldkamp, E., 2017. Gross N_2O emission and gross N_2O uptake in soils under temperate spruce and beech forests. Soil Biol. Biochem. 112, 228–236. https://doi.org/10.1016/j.soilbio.2017.05.011.

White, J.W., Hoogenboom, G., Stackhouse Jr., P.W., Hoel, J.M., 2008. Evaluation of NASA satellite-and assimilation model-derived long-term daily temperature data over the continental US. Agric. For. Meteorol. 148, 1574–1584.

White, J.W., Hoogenboom, G., Wilkens, P.W., Stackhouse Jr., P.W., Hoel, J.M., 2011. Evaluation of satellite-based, modeled-derived daily solar radiation data for the continental United States. Agron. J. 103, 1242–1251.

Xia, Y., Wander, M., 2022. Management zone-based estimation of positive and negative nitrous oxide flux in organic corn fields. Soil Sci. Soc. Am. J. 86, 1043–1057. https://doi.org/10.1002/saj2.20416.

Zeppetello, L.R.V., Cook-Patton, S.C., Parsons, L.A., Wolff, N.H., Kroeger, T., Battisti, D. S., Bettles, J., Spector, J.T., Balakumar, A., Masuda, Y.J., 2022. Consistent cooling benefits of silvopasture in the tropics. Nat. Commun. 13, 708. https://doi.org/10.1038/s41467-022-28388-4.

Zhang, K., Qiu, Y., Zhao, Y., Wang, S., Deng, J., Chen, M., Xu, X., Wang, H., Bai, T., He, T., Zhang, Y., Chen, H., Wang, Y., Hu, S., 2023. Moderate precipitation reduction enhances nitrogen cycling and soil nitrous oxide emissions in a semi-arid grassland. Glob. Change Biol. 29, 3114–3129. https://doi.org/10.1111/gcb.16672.

Zhao, Q., Guo, Y., Ye, T., Gasparrini, A., Tong, S., Overcenco, A., Urban, A., Schneider, A., Entezari, A., Vicedo-Cabrera, A.M., 2021. Global, regional, and national burden of mortality associated with non-optimal ambient temperatures from 2000 to 2019: a three-stage modelling study. Lancet Planet. Health 5, e415–e425.